

**Role of *DISTORTED2*, *GNARLED* and *SPIRRIG*
in cell morphogenesis of *Arabidopsis thaliana*.**

Inaugural-Dissertation

Zur
Erlangung des Doktorgrades
der Mathematisch-Naturwissenschaftlichen Fakultät
der Universität zu Köln

vorgelegt von

Rainer Saedler

aus Freiburg i. Br.

2005

Berichterstatter: Prof. Dr. Reinhard Krämer
Prof. Dr. Martin Hülskamp
Prüfungsvorsitzender: Prof. Dr. Ulf-Ingo Flügge

Tag der mündlichen Prüfung: 30. Mai 2005

Table of contents

Abbreviations and Gene names.....	III
List of figures.....	IV
1 Introduction	1
1.1 Microtubules during Cell Morphogenesis	4
1.2 Actin microfilament during Cell Morphogenesis.....	6
1.3 Molecular basis of actin cytoskeleton formation.....	8
1.4 Regulation of the ARP2/3 complex.....	10
1.5 Aim of the work.....	12
2 Material and Methods.....	13
2.1 Material.....	13
2.1.1 Chemicals, antibiotics.....	13
2.1.2 Enzymes and molecular biological materials	13
2.1.3 Cloning vectors.....	13
2.1.4 Vectors used for cytoskeleton labeling.....	13
2.1.5 Bacterial strains	13
2.1.6 Plant lines	13
2.1.7 Marker list	14
2.1.8 Primer list	14
2.2 Methods	16
2.2.1 RNA isolation.....	16
2.2.2 cDNA synthesis	16
2.2.3 Semiquantitative RT-PCR.....	16
2.2.4 Genomic plant DNA preparation.....	17
2.2.5 Plasmid DNA preparation from bacteria.....	17
2.2.6 DNA-manipulation	17
2.2.7 Mapping approach	17
2.2.8 TILLING Approach.....	17
2.2.9 Cloning of the <i>DIS2-1</i> cDNA	18
2.2.10 Cloning of the <i>GRL</i> cDNA	18
2.2.11 Cloning of the <i>SPI</i> cDNA.....	19
2.2.12 Plant growth conditions	19
2.2.13 Crossing of plants	19
2.2.14 Plant transformation	19
2.2.15 Seed sterilization	20
2.2.16 Drug treatments	20
2.2.17 Fluorescein diacetate staining.....	20
2.2.18 Microscopy	20
2.2.19 Sequence analysis programs.....	21

3	Results	22
3.1	The <i>DISTORTED2</i> (<i>DIS2</i>) gene	22
3.1.1	Identification of <i>DIS2</i> gene.....	22
3.1.2	Molecular characterization of <i>DIS2</i> gene	23
3.1.3	Phenotype of <i>distorted2-1</i>	25
3.1.4	Subcellular phenotype of <i>dis2-1</i> mutants	27
3.2	The <i>GNARLED</i> (<i>GRL</i>) gene	30
3.2.1	Molecular characterization of the <i>GRL</i> gene.....	30
3.2.2	Phenotypic characterization of the <i>grl</i> mutants	34
3.2.3	Subcellular phenotype of <i>grl</i> mutants.....	35
3.3	The <i>SPIRRIG</i> (<i>SPI</i>) gene	36
3.3.1	The <i>spirrig</i> mutant.....	36
3.3.2	Cloning of the <i>SPIRRIG</i> gene.....	36
3.3.3	Molecular characterization of <i>SPI</i>	38
3.3.4	Phenotypic characterization of the <i>spi</i> mutant.....	41
3.3.5	Subcellular phenotype of <i>spi</i> mutants.....	44
4	Discussion.....	45
4.1	<i>DISTORTED2</i> , a component of the ARP2/3 complex	45
4.1.1	The <i>distorted2</i> mutant phenotype	46
4.1.2	Localized growth	46
4.1.3	Cortical actin mesh.....	47
4.1.4	Possible interaction of cortical actin and microtubules.....	48
4.1.5	Cell growth	49
4.2	<i>GNARLED</i> , a potential regulator of the ARP2/3 complex.....	51
4.2.1	<i>grl</i> mutant phenotype.....	54
4.3	<i>SPIRRIG</i> , an unknown component in cell shape regulation	55
4.3.1	<i>Spirrig</i> mutant phenotype	55
4.3.2	Identification of the <i>SPI</i> gene	57
4.3.3	BEACH mutants in <i>Dictyostelium discoideum</i>	58
4.3.4	Putative <i>SPIRRIG</i> protein function in <i>Arabidopsis thaliana</i>	59
4.3.5	BEACH protein organization	60
	Abstract.....	62
	Zusammenfassung	63
	References	64
	Danksagung	75
	Erklärung	76
	Lebenslauf	77

Abbreviations and Gene names

°C	degree Celsius	k	kilo
μ	micro	kb	kilo bp
35S	35S promoter from Cauliflower Mosaic virus	kD	kilo Dalton
ARP2/3	Actin related protein 2 and 3	KLK	KLUNKER
ALI	ALIEN	<i>Ler</i>	Landsberg <i>erecta</i>
ATP	Adenosine triphosphate	min	minute
bp	base pair	mRNA	messenger RNA
C	DNA-content of a haploid genome	MT	microtubules
cDNA	complementary DNA	n	number
CLSM	confocal laser scanning microscopy	ORF	open reading frame
Col	Columbia	PCR	polymerase chain reaction
CRK	CROOKED	p	promoter
D	Dalton	RNA	ribonucleic acid
DIS1	DISTORTED1	rpm	rounds per minute
DIS2	DISTORTED2	RT-PCR	reverse transcription PCR
DNA	Deoxyribonucleic acid	SD	standard deviation
e.g.	<i>exempli gratia</i> (Lat.) for example	sec	second
EMT	endoplasmic microtubules	SPI	SPIRRIG
<i>et al.</i>	<i>et alterni</i> (Lat.) and others	T-DNA	transferred DNA
FDA	fluorescein diacetate	WT	wild type
Fig.	Figure	WRM	WURM
GFP	green fluorescent protein	YFP	yellow fluorescent protein
GRL	GNARLED		

All gen- and mutant names are written in italics. WT-genes are written in capital letters. Proteins are written in non-italic letters.

List of figures

Figure 1.	Cellular plant architectures.....	1
Figure 2.	Trichome development.....	3
Figure 3.	Schematic display of phenotypes caused by actin (red) and microtubule (blue) cytoskeleton defects in model cell types.....	6
Figure 4.	Models of the ARP2/3 complex.....	9
Figure 5.	WAVE/SCAR regulation pathways of the ARP2/3 complex.....	10
Figure 6.	Primary structure of the <i>DISTORTED2</i> gene.....	24
Figure 7.	The derived amino acid sequence for <i>DISTORTED2</i> aligned with protein sequences of the ARPC2 subunit of ARP2/3 complexes from reference organisms.....	25
Figure 8.	Comparison of leaf trichomes morphology in wild-type <i>Arabidopsis thaliana</i> (ecotype Landsberg <i>erecta</i>) and <i>distorted 2-1</i> mutant.....	26
Figure 9.	Actin and microtubule organization in <i>Arabidopsis thaliana</i> wild-type (Landsberg <i>erecta</i>) and mutant trichomes.....	27
Figure 10.	Molecular characteristics of the <i>GRL</i> gene.....	30
Figure 11.	Amino acid sequence comparison of the <i>Arabidopsis thaliana GRL</i> gene product with NAP125 from animal species.....	32
Figure 12.	Phenotypic characterization of <i>grl</i> mutants.....	34
Figure 13.	<i>SPI</i> mapping flowchart.....	37
Figure 14.	Molecular characterization of the <i>SPIRRIG</i> gene.....	39
Figure 15.	RT-PCR analysis of different <i>spirrig</i> alleles.....	40
Figure 16.	Schematical drawing of the putative SPI protein.....	41
Figure 17.	Phenotypic characterization of <i>spi</i> mutants.....	43
Figure 18.	Schematical drawing of a view through a cell.....	50
Figure 19.	Schematical drawing of proposed pathways for ARP2/3 regulation in plants.....	53
Figure 20.	Phylogenetic tree of BEACH proteins.....	59

1 Introduction

Plants feature a tremendous and almost unlimited diversity in architecture. Multi-cellular plants are quite diverse in their three-dimensional structure, e.g. *Sequoia gigantea*, *Zea mays* and *Arabidopsis thaliana*. In addition, their overall three-dimensional structure is made up of a variety of different cell forms. The shape of a cell can vary from simple roundish shapes to more complex architectures as demonstrated by round egg or pollen cells (Figure 1A); filamentous pollen tube cells (Figure 1B); bent or sausage-like guard cells (Figure 1C); cylindrical epidermal, hypocotyl (Figure 1D) or palisade cells, and highly lobed leaf epidermal cells (Figure 1E). The most extraordinary singularity in architecture is found in leaf epidermal trichomes with their stellar outgrowth (Figure 1F).

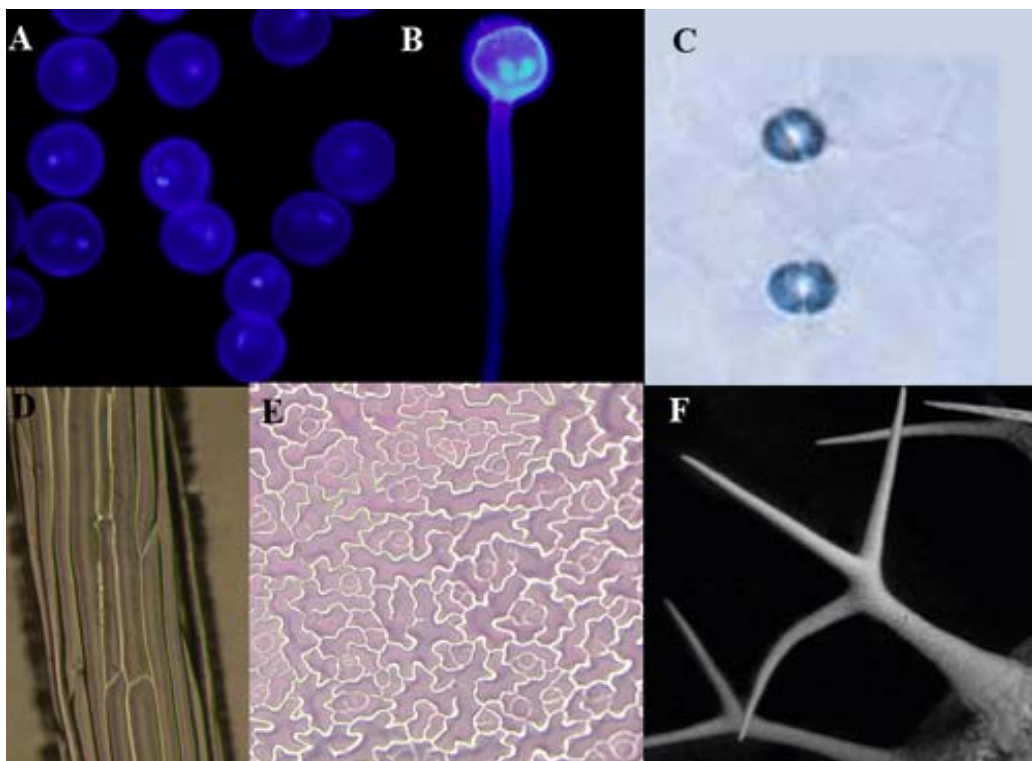


Figure 1. Cellular plant architectures. (A) DAPI stained pollen tube. (B) DAPI stained elongating pollen tube (A and B modified from Tansengco *et al.* 2004). (C) stained stomata cells (modified from von Groll and Altmann 2001). (D) agarose imprints of hypocotyl cells. (E) agarose imprints of epidermal pavement cells. (F) Leaf epidermal trichome (C-F *Arabidopsis thaliana*).

Based on the assembly of single constituent cells and their genetically and environmentally defined developmental frameworks, the architectural diversity of whole plants is accomplished. On a cellular level, all cells derive from a spherical precursor cell, but up to date, little is known about how a spherical cell is transformed into any other cell shape and especially about the underlying regulatory mechanisms.

In order to maintain its isodiametric shape, the cell must grow at every point of the membrane simultaneously and with similar velocity (Mathur 2004). In contrast, if cells grow in defined areas they will change their overall shape and thus increase their architectural complexity. This phenomenon is summarized in the term ‘differential growth’. In any case tight and precise regulation is required, which is achieved and fine-tuned through a molecular hierarchy of cellular components.

Differential cell growth has been studied using model cell types of *Arabidopsis thaliana*, such as epidermal pavement cells and leaf epidermal trichomes (Mathur and Hülskamp 2002, Hülskamp 2004), stomatal guard cells (Nadeau and Sack 2003), root-hair cells (Carol and Dolan 2002), elongating pollen tubes (Hepler *et al.* 2001) and differentiating tracheids (Fukuda 2004) that are readily accessible, easy to manipulate in experiments, and known for their pertinent morphological mutants. Although these cells differ greatly in their final shape, they do share underlying growth mechanisms (Mathur and Hülskamp 2002). Depending on their final destination cells can increase their volume by two broad categories: tip growth and diffuse growth, which differ in the membrane area where growth occurs. An essential component in cell growth is the turgor pressure from the vacuole (Smith 2003), which is a major component in plant cells.

Root hairs and pollen tubes are tip growing cells. During their development, they exhibit focused growth in a narrow region, which creates the typical rod-shaped cellular tip (Carol and Dolan 2002, Hepler *et al.* 2001). On the other hand, most root and hypocotyl cells, as well as the leaf epidermal trichomes grow diffusely over a large area of the cell surface (Mathur and Hülskamp 2002, Hülskamp 2004). Developing leaf epidermis pavement cells, however, most probably create their characteristic jigsaw-shape by a combination of those two growth modes (Fu *et al.* 2005).

Among the above mentioned cell types, leaf epidermal trichomes of *Arabidopsis thaliana* are particularly well suited as a model system because of their constant development into their characteristic three-dimensional form. These trichomes are unicellular, with precisely

angled branches, and they develop through a well-coordinated sequence of morphogenetic events (Figure 2 A-E) (Hülskamp *et al.* 1994; Folkers *et al.* 1997; Szymanski *et al.* 2000). After branch initiation, the trichome cell undergoes rapid elongation, ultimately producing a stellate, 350- to 500- μm -tall cell that is oriented perpendicular to the plane of growth. The enlargement of the cell is correlated with the DNA content in the nucleus. The cell undergoes three rounds of endoreduplication, which results in a 32C DNA content in the mature trichome nucleus. The predictability of trichome cell development, the distinct growth pattern, as well as the isolated position on the leaf surface provide excellent prerequisites to isolate mutants affecting discrete aspects of trichome morphogenesis (Hülskamp *et al.* 1994).

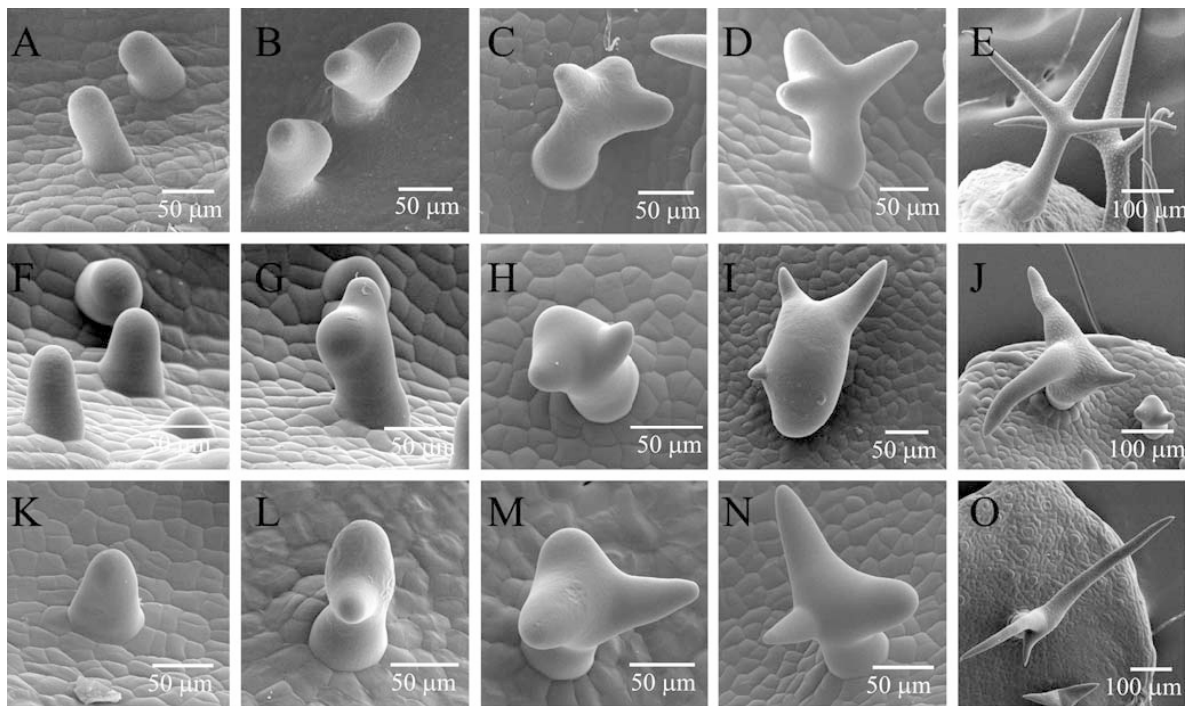


Figure 2. Trichome development. (A–O) Different stages of developing wild type and distorted mutant trichomes observed with a scanning electron microscope. (A–E) Wild type. (F–J) *crk* (ARP2/3) mutant. (K–O) *spi* mutant. Pictures in the first three columns show developmental stages of trichomes from incipient to three branched stages. The pictures in the fourth column display trichomes in the rapid growth phase in which the distortion is pronounced. The last pictures in the rows show mature trichomes. (modified from Schwab *et al.* 2003)

In an ethyl-methanesulfonate (EMS) mutagenesis screen, eight complementation groups were identified (*alien*, *crooked*, *distorted1*, *distorted2*, *gnarled*, *klunker*, *spirrig*, and *wurm*) by a common “distorted” trichome phenotype and characterized on the genetic level (Hülkamp *et al.* 1994). The beginning of mutant and wild type trichome development is similar (Figure 1) but in the rapid growth phase, after branch initiation, the distortion of the shape becomes clearly visible (Schwab *et al.* 2003) (Figure 2 F-O) indicating that the morphological cell aberration observed in the ‘*distorted*’ class mutants depends on alterations of cell growth.

The cell growth process, as shown in various studies on different cell types, is greatly depending on cytoskeletal elements that play roles as transducers, scaffolds and transporting tracks (Wasteneys 2002). Perusal of numerous snapshot studies on cytoskeletal involvement in plant cell morphogenesis reveals two basic cell shape alterations: a) those created by microtubule defects, where anisotropically growing cells shift into an isotropic growth mode to acquire a more expanded, rounded appearance, and b) those where actin defects prevent proper cell expansion and result in short, deformed cells (Mathur and Hülkamp 2002). The interaction of cytoskeletal players, actin and microtubule to form cell shape is essential, but how this is achieved remains still unclear.

1.1 Microtubules during Cell Morphogenesis

Microtubules are often found to align with wall microfibrils in reverse orientation to the direction of cell expansion. Microtubule orientation is thus believed to determine the direction of growth through deviations in microtubule–microfibril co-alignment (Giddings and Staehelin 1991, Baskin 2001).

This is supported by experiments using microtubule interacting drug treatments in diffuse growing cells. Leaf epidermis, hypocotyl, and primary root cells with impaired microtubules swell isotropically suggesting that the cells grow but lose their directionality (Baskin *et al.* 1994). Anisotropically growing leaf trichomes, which are usually branched, lose their branching capability and appear in a globular shape (Figure 3) upon drug treatment (Mathur and Chua 2000).

In tip-growing root hair cells the effect is even more striking. Under regular conditions a single trichoblast gives rise to one root hair (Schneider *et al.* 1997) whereas under

treatment with microtubule drugs one trichoblast initiates and forms multiple root hairs (Bibikova *et al.* 1999). These observations imply that the microtubules are involved in the selection of an area, in which focused tip growth occurs.

Mutants harboring defects in microtubule-associated genes show an abnormal swelling of diffusely growing cells such as trichomes, root, hypocotyl and pavement cells, whereas tip-growing root hairs usually become sinuous or branched. These cellular defects are found in some mutants of the *ZWICHEL* gene, encoding for a kinesin-like microtubule motor protein (Oppenheimer *et al.* 1997), in weak mutant alleles of the *KIESEL* or *PORCINO* genes encoding for tubulin-folding cofactors (Kirik *et al.* 2002a, Kirik *et al.* 2002b), and in the mutant of *MOR1/GEMIN1* encoding a XMAP215 homolog (Whittington *et al.* 2001, Twell *et al.* 2002).

Another link to the microtubule cytoskeleton has also been proposed based on the mutant phenotypes of the *ANGUSTIFOLIA* (Folkers *et al.* 2002, Kim 2002) and *SPIKE1* genes (Qiu *et al.* 2002) in which polarized growth is effected by loss of branch points. In general, all microtubule cytoskeleton-associated phenotypes suggest their involvement in cell polarization and maintenance of growth directionality.

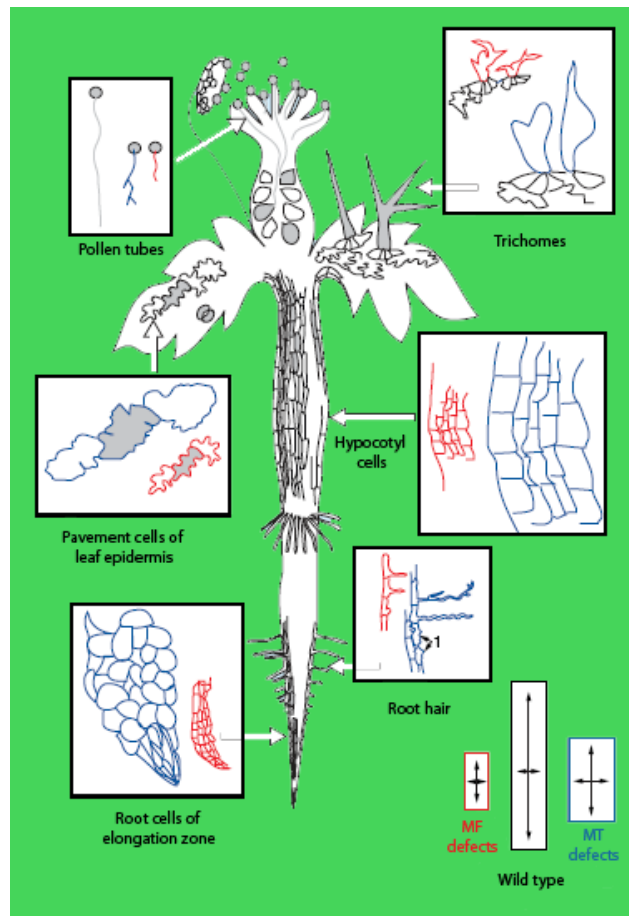


Figure 3. Schematic display of phenotypes caused by actin (red) and microtubule (blue) cytoskeleton defects in model cell types. The three rectangles at the bottom of the figure depict the cytoskeleton-linked changes in cell size with the wild-type cell (middle). In general actin cytoskeleton defects result in reduced cell elongation/expansion. Microtubule defects lead to loss of growth focus, increased expansion and a general rounding up of the cell shape. (modified from Mathur and Hülskamp 2002).

1.2 Actin microfilament during Cell Morphogenesis

Initial investigations of phenotypes caused by mutations in actin-encoding genes in *Arabidopsis thaliana* did not reveal apparent morphological cells defects. Recent studies suggested a high degree of functional redundancy of these essential genes as an explanation (Meagher *et al.* 2000). However, treatments with actin microfilament interacting drugs disclosed drastically reduced cell expansion. For instance, treatments of seedlings with the actin polymerization inhibitor latrunculin yield small, dwarfish plants (Baluska *et al.* 2000), in which leaf epidermis, root, and hypocotyl cells remain relatively

small and unexpanded. Similarly, root hairs and pollen tubes do not elongate properly and remain short and stubby (Baluska *et al.* 2000, Hepler *et al.* 2001) (Figure 3).

Drug treatment reduces leaf epidermal trichomes in size and leads to a distorted phenotype. The initiation of trichome branches is unaffected, even if branches do not elongate properly. In most cases, trichome distortion can be traced back to aberrant actin organization (Mathur *et al.* 1999; Szymanski *et al.* 1999) indicating that the actin inhibitors can phenocopy the *distorted* mutant cell shape. All *distorted* mutants, except one member, namely *spirrig*, harbor altered actin cytoskeletons (Mathur *et al.* 1999; Szymanski *et al.* 1999, Schwab *et al.* 2003).

In all growing plant cells several types of actin arrays can be detected that are likely to carry out different functions. Heavily bundled actin filaments, for example, are commonly observed throughout the cytoplasm and in transvacuolar strands in growing plant cells. These microfilaments provide a scaffold to orientate the endoplasmic reticulum (Boevink *et al.* 1998) and to maintain conduits for long-distance organelle transport. By using dual labeling strategies it was shown that, contrary to animals, organelles such as chloroplasts (Sheahan *et al.* 2004), peroxisomes (Mathur *et al.* 2002), and Golgi stacks (Nebenfuhr *et al.* 1999) traffic on actin bundles. An efficient long-distance transport may control the organelles inheritance (Sheahan *et al.* 2004) and the distribution of organelles to support local metabolic needs. Actin filaments mediate short-range recycling of endosomal compartments, such as those in which the auxin efflux carrier resides (Geldner *et al.* 2001). Plant cells also contain cortical actin filaments that are in close proximity to the plasma membrane. In many cell types, regions of active cell expansion correlate with the presence of fine networks of actin filaments and supposedly support cell growth (Mathur 2004).

Based on drug treatments interacting with the actin cytoskeleton, the movement of organelles in the long and short distance traveling could be altered and also in some cases arrested (Hawes and Satiat-Juenemaitre 2001, Mathur *et al.* 2002, Van Gestel *et al.* 2002). This distortion in the actin cytoskeleton may therefore cause a reduced as well as misdirected delivery of different vesicles to the cell cortex resulting in growth reduction and cellular distortion. As actin-drug-treated cells show no initial defects in growth directionality, the actin cytoskeleton does not appear to be involved in establishment or maintenance of growth directionality directly.

1.3 Molecular basis of actin cytoskeleton formation

The actin cytoskeleton consists of actin filaments (F-Actin), which are directional polymers that preferentially add globular actin (G-actin) subunits to their barbed (plus) ends, and tend to lose subunits from their pointed (minus) ends. F-Actin filaments are dynamic and vary with respect to their stability as well as the extent of bundling. In all organisms, the actin isoforms themselves contribute to organ and cell-type-specific functions of the actin cytoskeleton (Gilliland *et al.* 2003, Kandasamy *et al.* 2002, Ringli *et al.* 2002). However, the spontaneous nucleation process of actin to actin filaments is slow. Thus, eukaryotic cells have several classes of proteins, important for formation and stability of actin filaments. These controlling proteins are factors that affect actin nucleation, actin monomer sequestration, actin polymerization and depolymerization kinetics (Welch and Mullins 2002).

One of the protein complexes that initiate actin polymerization from the pool of G-actin monomers is the actin related protein 2 and 3 (ARP2/3) complex. The ARP2/3 complex was first identified in *Acanthamoeba castellanii* (Machesky *et al.* 1994) and is now known from diverse organisms (Vartiainen and Machesky, 2004). Out of seven known subunits that form the complex (ARP2, ARP3, ARPC1 (p40 yeast homolog), ARPC2 (p34), ARPC3 (p21), ARPC4 (p20), and ARPC5 (p16)) two, namely ARP2 und ARP3, resemble actin in sequence and structure (Robinson *et al.* 2001) (Figure 4). This observation led to the hypothesis that these two proteins form a stable actin-like dimer within the complex as a template for the nucleation of new F-actin filaments (Volkman *et al.* 2001). In the presence of a specific activating protein, the complex interacts with an existing filament and initiates a new filament at a precise angle of 70 degrees relative to the parental filament (Mullins *et al.* 1998, Blanchoin *et al.* 2000). The ARP2/3 complex initiates filaments from the flanks of mature filaments (Blanchoin *et al.* 2000) although there is some evidence that the branches can also originate from the barbed end of filaments (Carlier *et al.* 2003).

Recent publications, based on the analysis of *distorted* mutants, demonstrated that this complex exists in plants as well. The *WURM* (*WRM*) gene and the *DISTORTED1* (*DIS1*) gene encode homologues of the ARP2 and ARP3 subunits, respectively (Le *et al.* 2003, Li *et al.* 2003, Mathur *et al.* 2003a). The *CROOKED* (*CRK*) gene encodes a protein with sequence similarity to ARPC5 (Li *et al.* 2003, Mathur *et al.* 2003b).

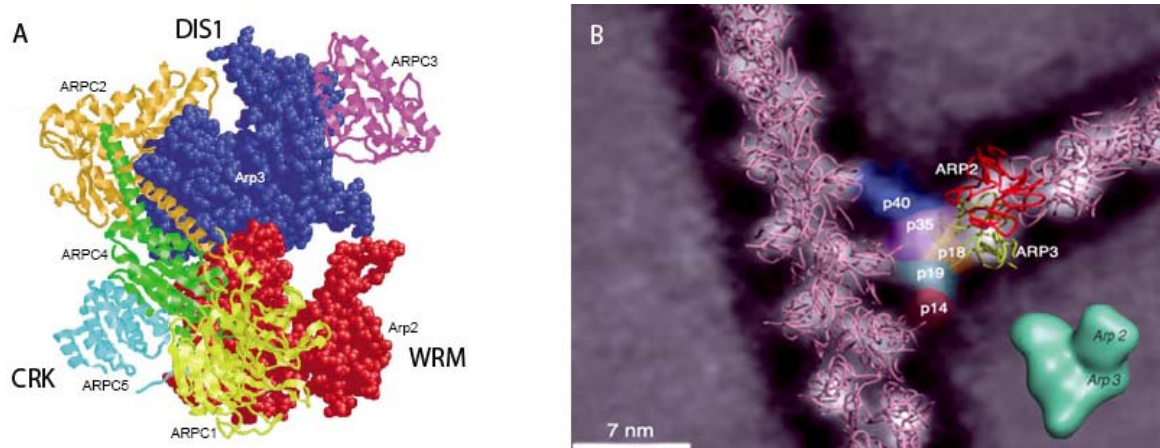


Figure 4. Models of the ARP2/3 complex. A) Model of the inactive ARP2/3 complex based on crystal structures, indicating ARP2, ARP3, and the five subunits ARPC1-5. In large font, the homologues in plants DISTORTED1, CROOKED, and WURM are marked (modified from Winder 2003). B) Model of actin filament branches mediated by the *Acanthamoeba castellanii* ARP2/3 complex. ARP2 (red) and ARP3 (yellow) are also represented in the lower corner; they serve as actin nucleation points. The five subunits are attaching the mother filament. The barbed ends of the filaments are oriented towards the top of the Figure (modified from Volkmann *et al.* 2001).

Contrary to all non-plant organisms, in which the loss of some ARP2/3 subunits is lethal (Winter *et al.* 1999, Hudson and Cooley 2002, Stevenson *et al.* 2002, Zallen *et al.* 2002, Sawa *et al.* 2003, Yan *et al.* 2003), all null ARP2/3 mutations in plants exhibit a mild mutant phenotype. The plants are vigorous but have a modest reduction in shoot fresh weight; seed set is normal as well as the overall plant architecture. Tip-growing cells, such as pollen tubes that have a strict growth requirement for the actin cytoskeleton, do not show clear mutant phenotypes. The length of etiolated hypocotyls and the size of epidermal cells are reduced relative to those of the wild type (Mathur *et al.* 2003a). In both, the hypocotyl (Mathur *et al.* 2003a) and cotyledon epidermis (El-Assal *et al.* 2004, Le *et al.* 2003, Li *et al.* 2003), clear gaps between adjacent cells have been observed in these mutants.

1.4 Regulation of the ARP2/3 complex

In animals and yeast, the ARP2/3 complex is activated locally in growth regions where it triggers actin branching (Welch *et al.* 1997, Winter *et al.* 1997). A plethora of regulatory proteins is known that interact with the ARP2/3 complex and control its site-specific activity. The ARP2/3 complex itself is inactive but two pathways are known to regulate, respectively activate, the ARP2/3 pathway. In the first pathway the ARP2/3 complex is activated by the Wiskott–Aldrich syndrome protein (WASP). WASP is an auto-inhibited protein; its physical interaction with the small GTPase CDC42 and with phosphatidylinositol 4, 5-bisphosphate allows the protein to activate the ARP2/3 complex (Rohatgi *et al.* 2000) (Figure 5).

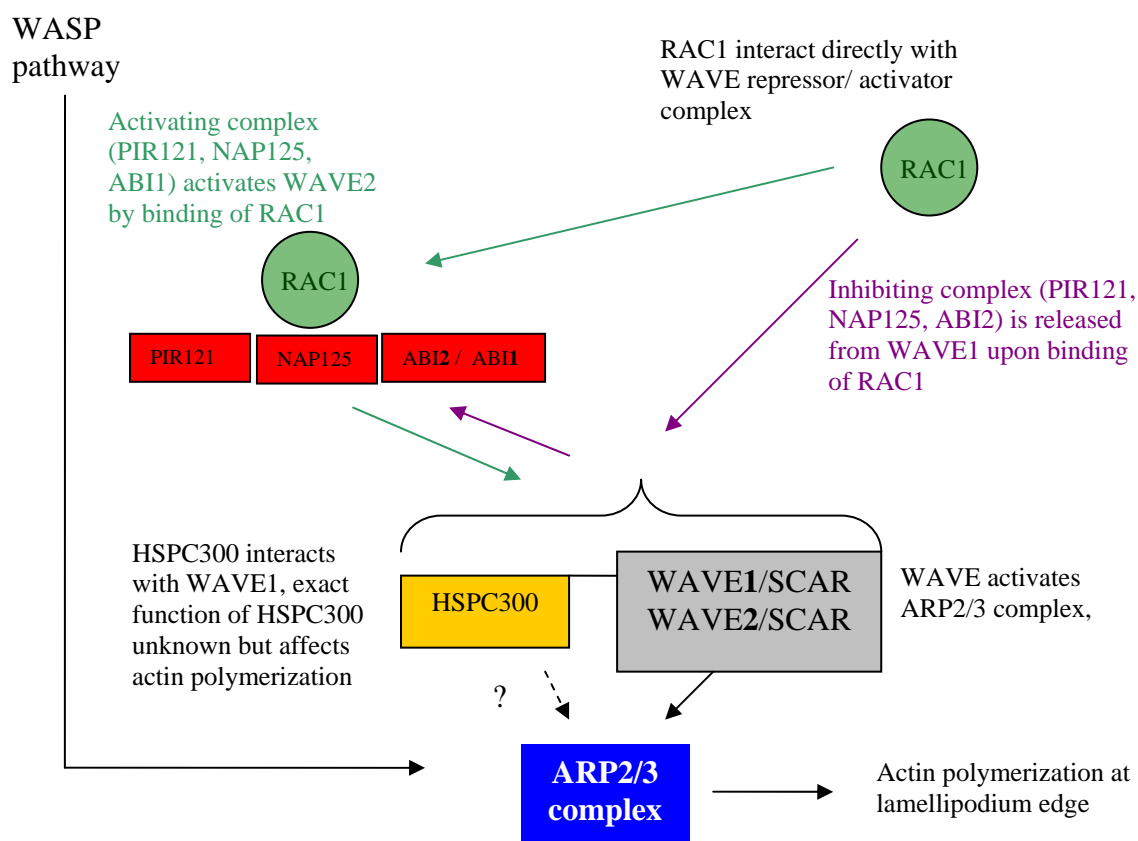


Figure 5. WAVE/SCAR regulation pathways of the ARP2/3 complex. Hypothetical interaction is drawn as dashed line; proven interactions are drawn as solid lines. Green lines suggest activation, purple lines inactivation.

The second pathway is regulated by the small GTPase RAC1, which activates WAVE/SCAR (Wiskott-Aldrich syndrome protein family verprolin-homologous protein/suppressor of cAMP receptor defects) and HSPC-300 (hematopoietic stem/Progenitor cell clone 300) upon GTP binding through another protein complex. The WAVE/SCAR/HSPC-300 complex then activates the ARP2/3 complex.

In both pathways, the ARP2/3 complex is activated by the verprolin-cofilin-acidic (VCA) region of WAVE/SCAR and WASP proteins (Machesky and Insall 1998). The verprolin domain binds an actin monomer, whereas the cofilin/central domain interacts with the ARP2/3 complex (Higgs *et al.* 1999, Panchal *et al.* 2003) to induce filament branch formation.

In the WAVE/SCAR regulatory pathway, two controlling scenarios are found. As some WAVE/SCAR proteins are intrinsically active (Machesky *et al.* 1999), they are inhibited through a ternary complex consisting of NAP125 (NCK-associated protein), Abi2 (Abl interactor 2) and PIR121 (p53-inducible messenger RNA), which is an isoform of SRA1 (Eden *et al.* 2002, Blagg and Insall 2004). Binding of RAC1 releases this complex (Eden *et al.* 2002) facilitating WAVE1-mediated activation of the ARP2/3 complex (Eden *et al.* 2002) (Figure 5).

A second scenario is found in which a different set of proteins regulate the ARP2/3 complex as well. WAVE2, however, appears to be activated by Abi1, NAP125, and PIR121, and re-localizes by interaction with RAC1, thereby locally activates the ARP2/3 complex (Miki *et al.* 2000, Blagg and Insall 2004, Innocenti *et al.* 2004) (Figure 5).

At the beginning of this thesis, the WASP and WAVE/SCAR pathways were unknown in plants. Indication that a WAVE/SCAR pathway exists where given by the observation that several plant-specific Rho-like GTPases, so-called ROPs, (RAC GTPases in animals) were involved in actin-dependent cell shape regulation suggested the existence of a similar pathway in plants (Mathur and Hülskamp 2002, Yang 2002).

1.5 Aim of the work

Many important questions about the molecular mechanisms of plant cellular growth remain unresolved so far. Actin microfilaments seem to be the key factor for local growth. Alterations of trichome morphologies in defined mutants like the “distorted class”, in which some members harbor defects in the ARP2/3 complex, show an aberrant actin cytoskeleton. The ARP2/3 complex triggers actin nucleation and branching and therefore participates directly in the assembly of the actin cytoskeleton. Out of the distorted group, three members encode subunits of the ARP2/3 complex. As this complex seems to be functionally conserved among Eukaryotes, other members of the *distorted* group might encode further subunits or proteins in the regulatory pathway.

Three morphological mutants, *distorted2*, *gnarled* and *spirrig*, out of the *distorted* mutant group, exhibiting trichome phenotypes of different strength, were selected to investigate whether and how they affect the ARP2/3 dependent regulation of the actin cytoskeleton. The mutant *spirrig*, described as the only *distorted* mutant without an aberrant actin cytoskeleton, was chosen to investigate its involvement in cell shape alteration. These three genes could encode for a novel pathway of how cell shape is achieved. For that purpose the genes had to be cloned and identified. Furthermore, the function of the three genes, based on a phenotypical description of the corresponding mutants, had to be analyzed in detail.

2 Material and Methods

2.1 Material

2.1.1 Chemicals, antibiotics

All chemicals and antibiotics were purchased from Sigma (Deisenhofen), Roth (Karlsruhe) and Appligene (Heidelberg) in p.a. quality.

2.1.2 Enzymes and molecular biological materials

Restriction enzymes were supplied by MBI-Fermentas (St.Leon-Rot), New England Biolabs (Frankfurt/Main) and Roche (Mannheim). Oligonucleotides were synthesized by Sigma-ARK Scientific, biomers.net GmbH (Ulm) and Invitrogen (Karlsruhe).

2.1.3 Cloning vectors

pGEM-T easy (Promega) for PCR-product cloning,

pBIN19 containing the GLABRA2 promoter and kanamycin resistance (Szymanski *et al.* 1998).

2.1.4 Vectors used for cytoskeleton labeling

GFP-mTalin and GFP-MAP4 constructs (Kost *et al.* 1998, Marc *et al.* 1998).

2.1.5 Bacterial strains

For standard cloning procedures were performed using *Escherichia coli* strains DH5a and XL-10 gold. For plant transformation the *Agrobacterium tumefaciens* strain GV3101 was used.

2.1.6 Plant lines

Two *Arabidopsis thaliana* ecotypes were used in this study: Landsberg *erecta* (Ler) and Colombia (Col). The EMS generated alleles of *spirrig* (*spi-11*, *spi-4.2*, *spi-12* and *spi-139*)

(Hülskamp *et al.* 1994), *gnarled* (*grl-EM1* and *grl-EM2*) (Hülskamp *et al.* 1994) and *dis2-1* (Feenstra 1978) were in a *Ler* background. The Gabi-Kat line (Rosso *et al.* 2003) and the SALK lines (Arabidopsis Biological Resource Center (Ohio State University, Columbus, OH, USA)) were in Col background.

2.1.7 Marker list

Marker name	COL	LER	
RSM T7I23_1	303 bp	258 bp	
RSM F10O3_1	282 bp	234 bp	
RSM F12K11_1	200 bp	155 bp	
RSM T7A14_1	250 bp	189 bp	
RSM T1G11_1	280 bp	259 bp	
RSM F21M11_1	186 bp	176 bp	
RSM F21B7_1	200 bp	179 bp	
RSM F22D16_1	152 bp	143 bp	
RSM F22D16_2	199 bp	191 bp	
RSM F10O3_2	158 bp	149 bp	
RSM T14P4_2	396 bp	390 bp	
RSM F22D16_3	290 bp	282 bp	
RSM F10O3_3	327 bp	344 bp	Apa I
RSM F10O3_4	309 bp	290 bp	Hae III

2.1.8 Primer list

RS1_NGA59_1	5`	TTAATACATTAGCCCAGACCCG	3`
RS2_NGA59_2	5`	GCATCTGTGTTCACTCGCC	3`
RS3_NGA63_1	5`	ACCCAAGTGATCGCCACC	3`
RS4_NGA63_2	5`	AACCAAGGCACAGAAGCG	3`
RS13_T7I23_1	5`	AAAATGGACGAAATGAGATG	3`
RS14_T7I23_2	5`	TCACAACCTATGGGTCTGACT	3`
RS15_F10O3_1	5`	GCATTGCATTTTGGATTAAC	3`
RS16_F10O3_2	5`	CCGAAAAATATCAAGTGTTGAC	3`
RS17_F12K11_1	5`	TAACCTGTAAAGCTCTTCC	3`
RS18_F12K11_2	5`	CTCGAATCTAACCAAATGTC	3`
RS34_T7A14_1	5`	ATGGTATGTGTTACTTAAGCC	3`
RS35_T7A14_2	5`	AGTCATTCATTATGCCTTTG	3`
RS36_T1G11_1	5`	AGCCTAAGTTCCTCGGCTTCCTTGATAT	3`
RS37_T1G11_2	5`	CCATGGAAGTGTGATATCAAAGTTGTTACA	3`
RS38_F21M11_1	5`	ACGTTTTATTGAATCCGCAT	3`
RS39_F21M11_2	5`	AAACTTGCGCCGAAAGAATC	3`
RS40_F21B7_1	5`	TTTCTGCCTCTGTTCTTCATCTT	3`
RS41_F21B7_2	5`	CCAAGAAAGACTTCACCGAT	3`
RS42_F22D16_1	5`	ACATACAAAGCAGTGAAGA	3`
RS43_F22D16_2	5`	AGAGACCATCAATAAGGATG	3`
RS66_F22D16_1	5`	CTTGGATTCCGAGTCCTAAA	3`
RS67_F22D16_2	5`	CTGCTCTTCAATAATATAAGGAGAG	3`
RS68_F10O3_1	5`	TATGAATCGCGAAAAGGGGA	3`
RS69_F10O3_2	5`	GCGTTCATCAATGGAGGTTT	3`
RS84_F16D14	5`	TTGGGACAACAAGGATCACTC	3`
RS85_F16D14	5`	TAGACCAACAACACCATTCCG	3`
RS86_F16D14	5`	ACTTTTAGTATCTGACATTGCTTGGC	3`

RS87_F16D14	5`	AATAAAGGTGGATGCTGACCC	3`
RS88_F16D14	5`	TTTTACTTTTGAGAACCTGG	3`
RS89_F16D14	5`	AGCTGACTACTGATCCAGAT	3`
RS90_F7F1	5`	CACATGAGAACAACCTTTCTCAAAG	3`
RS91_F7F1	5`	CCTGAATTGATATATTATCGGG	3`
RS92_F7F1	5`	GTGAGCCAGAATTGTTTTATTTGTGTG	3`
RS97_F7F1_4	5`	AGTTACTCTATACTCATAGACTCATAGTGAG	3`
RS98_F16D14_7	5`	GTAACTTATTTGGGATTTCG	3`
RS99_F16D14_8	5`	AAGAAAACCATGGGGATCGACCAGG	3`
RS100_F16D14_9	5`	CGGTTCAACCGAAGCACTAATCTTT	3`
RS101_F16D14_10	5`	AAAAGGTTTTATCAGATTCTCTTCAGTGACACCCAATAAG	3`
RS102_F16D14_11	5`	GGTTGTGATTGAGAAACAGGGTTTT	3`
RS103_F16D14_12	5`	AAGATTCGTGCCTTTTCCGG	3`
RS104_F16D14_13	5`	CAGGGCCAAGGAAAATAGAA	3`
RS105_F7F1_5	5`	GTTTGCCCAAAAATAAAGGTCCA	3`
RS106_F7F1_6	5`	CACAAAGTGCAGCAGCATT	3`
RS107_F7F1_7	5`	TGTATTCTGAGCTGTTTCATTCTTA	3`
RS108_F7F1_8	5`	GACAGTAGTTGTTTTGCAATAAGTGAGA	3`
RS109_F7F1_9	5`	ATGACCTAACCATGTTTGTGTTGTT	3`
RS110_F7F1_10	5`	GACAGTAGTTGTTTTGCAATAAGTGAGAAAC	3`
RS117_T14P4_3	5`	AGGTTCTTGAGGAAGAATCAGAGTGTG	3`
RS118_T14P4_4	5`	TTTCAAATCGAGACGGAACATAGT	3`
RS119_F22D16_3	5`	ACTTCATTGGTTCCTTGGATTCCGAG	3`
RS120_F22D16_4	5`	CCGAAATATACCGCGGATCAATCTCTAG	3`
RS139_F10O3_5	5`	ATATATGTTAGCATTTTACATTAG	3`
RS140_F10O3_6	5`	TAATTCTTTTACAAATGGGG	3`
RS141_F10O3_7	5`	ATGATCACTTCTTCCTTGGC	3`
RS142_F10O3_8	5`	CGATCAGTTCTACTCTTGGT	3`
RS296	5`	CACCATGAAATGGGCAACATTGC	3`
RS297	5`	GCGGCGGGCGCGCCATCACATTTTCGCATCATCATGAA	3`
RS300	5`	GGAATGGTCACTGGTATTTCTGGCC	3`
RS301	5`	GCGGCGGGCGCGCCTAAGACAATGCAGTTTGAAGTTT	3`
RS303	5`	ATCTTAGTCTTTTCGAGGTTCCGG	3`
RS304	5`	GCGGCGGGCGCGCCATCAACATAGAAAGGAACCATTT	3`
RS306	5`	GATTTTATGGCAGAGGCACTTGCTG	3`
RS307	5`	GCGGCGGGCGCGCCTTTCTCCATTTTGCATCTTTT	3`
RS309	5`	GGAAAGTAACGAGGGAGGCC	3`
RS310	5`	GCGGCGGGCGCGCCTAAACCGATGAAGCCTGTT	3`
EF1aA4-UP	5`	ATGCCCCAGGACATCGTGATTTTCAT	3`
EF1aA4-RP	5`	TTGGCGGCACCCTTAGCTGGATCA	3`
grl _{fw}	5`	CACCATGGCGAATTCTCGTCAATAT	3`
grl _{rev}	5`	AGTCGGCGCGCCTTAGTTATGCTGTTTATATGAG	3`
act _{fw}	5`	TGCGACAATGGAAGTGAATG	3`
act _{rev}	5`	GGATAGCATGTGGAAGTGCATAC	3`
JM406	5`	GCGAAAGTAATCGATGATACTATTGCAG	3`
JM407	5`	TTAAAGCTTCCAACACTTTCGAGTTGGT	3`
JM408	5`	CGATGATACTATTGCAGTCACATTC	3`
JM409	5`	TAACACTTTCGAGTTGGTGTGATTG	3`

2.2 Methods

2.2.1 RNA isolation

Whole plants or plant organs were used to isolate RNA. Plant material was homogenized with a mortar and pestle under constant addition of liquid nitrogen. 1 ml Trizol (Molecular Research Center, Inc., Cincinnati, OH) was added per 100 mg of sample. After an incubation of 5 min at 25°C, 0.2 ml chloroform was added and samples were shaken for 15 sec. Additional incubation of 3 min at 25°C and centrifugation at 16000 g at 4°C followed. The aqueous (=upper) phase was collected and transferred into a new 1.5-ml-tube. After adding 500 µl isopropanol (samples were incubated (10 min, 25°C) and centrifuged (10 min at 16000 g, 4°C). The resulting gelatinous pellet was washed with ice cold 70% (v/v) ethanol. After vigorous vortexing the resuspended pellet was centrifuged (10 min, 16000 g, 4°C). The RNA pellet was briefly air dried (3-5 min) and resolved in 50 µl diethylpyrocarbonate-treated H₂O and incubated at 55-60°C for 10 min to ensure complete re-suspension.

2.2.2 cDNA synthesis

Reverse transcription was performed using the 'RevertAidTM H Minus First Strand cDNA Synthesis Kit' (Fermentas) following the instruction of the manufacturer.

2.2.3 Semiquantitative RT-PCR

The expression levels of *SPI* were quantified by semi-quantitative RT-PCR with primer pair RS197/RS198 and actin was used as control. For expression analysis of the GABI-Kat line the primer pair RS197/RS198 was used as a probe and the elongation factor 1 (primer pair EF1aA4-UP/EF1aA4-RP (Nesi *et al.* 2000)) as control. All RT-PCR analyses were done with 30 cycles.

2.2.4 Genomic plant DNA preparation

Genomic DNA for PCR analysis was prepared by using CTAB (Rogers and Bendich 1988).

2.2.5 Plasmid DNA preparation from bacteria

Plasmid preparation was performed using microcolumn-based pEQ-LAB Plasmid Miniprep Kit I (PEQLAB Biotechnology GmbH, Erlangen) according to the manufacturers protocol. Plasmid DNA from *Agrobacterium tumefaciens* was isolated using the Qiagen plasmid miniprep kit.

2.2.6 DNA-manipulation

DNA manipulation and cloning were carried out according to Sambrook and Russel (2001) or Ausubel *et al.* (1994). All polymerase-chain reaction (PCR)-amplified fragments were sequenced prior to further investigation. Sequencing was carried out on an ABI 310 Prism automated sequencer (Perkin-Elmer Applied Biosystems, Foster City, CA) according to the manufacturer's instructions. Sequencing reactions were performed using Big-Dye kit 1.1 or Big-Dye kit 3.1 (Perkin Elmer Applied Biosystems, Foster City, CA).

2.2.7 Mapping approach

Various molecular simple sequence length polymorphism (SSLP) or derived cleaved amplified polymorphic sequence (dCAPS) markers were used. SSLP markers are based on PCR length differences obtained from different templates (mutant and wild-type background). dCAPS markers were used to utilize single nucleotide alteration between different ecotype to create a primer with a digestion site in the one but not in the other ecotype. For marker details see marker list (2.1.7).

2.2.8 TILLING Approach

Tilling is a fast and easy method to detect single nucleotide mismatches in a DNA heteroduplex (Till *et al.* 2003).

1.6 Kb PCR products were generated by using 86 appropriate primers (sequence on demand). Templates from several EMS mutant backgrounds (*spi4.2*, *spi-11*, *spi12*, *spi139*) and the corresponding wild type background were used for PCR. The PCR was conducted to generate single strands after the exponential PCR amplification, by decreasing the temperature. Equal amounts of mutant and wild type PCR products were mixed to produce heteroduplex or homoduplex DNA fragments. To identify single nucleotide mismatches in heteroduplex DNA fragments, a restriction digest was performed with CEL 1 that

exclusively cuts heteroduplex PCR fragments at the mismatch site. Single polymorphism between mutant and wild-type were analyzed on a 1% agarose gel.

2.2.9 Cloning of the *DIS2-1* cDNA

For identification of the *DIS2* gene a genomic fragment of At1g60430 WT gene from Landsberg *erecta* genomic DNA of approximately 900-bp was cloned using the PCR primers JM217F/JM218R (2.1.8). For the Atg1g30825 gene the primers were JMF406/JM407R (genomic clone ca. 1,900 bp) and JM408F/JM409R (cDNA clone ca. 960 bp) were used to amplify the DNA (2.1.8). The respective genomic and cDNA fragments were sub-cloned into a pGEM-T-easy vector (Promega), sequenced, and finally re-cloned into a trichome specific *GLABRA2* promoter (Szymanski *et al.* 1998) for plant transformation using Hind III. Different transgenes were introduced into the *dis2-1* mutant (Landsberg *erecta* background; (Feenstra 1978) by genetic crossing or by *Agrobacterium tumefaciens* (strain GV3101)-mediated floral dip transformation (Clough and Bent 1998). For complementation through transient expression the BAC DNA (t17h7 containing the At1g30825 gene) was mixed with a green fluorescent protein (mGFP5) and precipitated on 1 µm diameter gold particles (BioRad, Hercules, CA, U.S.A.) following the manufacturer's directions. The particles were loaded onto carrier membranes and shot into 7- to 10-day-old seedlings at 1,100 psi Helium pressure under a vacuum of 25 inches of Hg, using a PDS-1000/Helium driven Biolistic delivery apparatus (BioRad). Following complementation of the trichome cell phenotype, genomic and cDNA achieved from amplification (JMF406/JM407R for the Atg1g30825 gene) of the *DIS2-1* gene was cloned into pGEM-T-easy vector (Promega) and subjected to sequence analysis.

2.2.10 Cloning of the *GRL* cDNA

The *GRL* gene was identified by sequencing the *Arabidopsis thaliana* NAP125 homolog (At2g35110) in several *grl* alleles. Information on the genomic sequence was obtained from the MIPS *Arabidopsis* database (<http://mips.gsf.de/cgi-bin/proj/thal/>). Genomic DNA and cDNA were obtained by using primer combination *grlfw* and *grlrev* (2.1.8). The genomic and cDNA fragments were cloned in the pGEM-T-Easy vector (Promega) and sequenced.

2.2.11 Cloning of the *SPI* cDNA

The *SPI* gene was identified by sequencing various 1600 bp genomic DNA fragments obtained from the tilling experiment. These sequences were compared with sequence data from the MIPS *Arabidopsis* database (<http://mips.gsf.de/cgi-bin/proj/thal/>). Due to its large size, the cDNA was subdivided into 5 parts and sequenced. The fragments were generated with the following primer pairs: Fragment 1 (RS296/RS297), fragment 2 (RS300/RS301), fragment 3 (RS303/RS304), fragment 4 (RS306/RS307) and fragment 5 (RS309/RS310) (2.1.8). The PCR fragments were either directly sequenced or cloned into the pGEM-T-Easy vector (Promega) and then sequenced.

2.2.12 Plant growth conditions

Seeds were sown on humid freshly prepared *Arabidopsis* culture soil. The trays were covered with a plastic lid and stored for two to three days at 4°C. Plants were grown under constant 16h light and 8h dark regime at a constant temperature of 22°C. The lid was removed after three to four days. Rapid hypocotyl growth was induced by growing the seedlings for 8 days under low-light conditions.

Plates containing seeds were wrapped with aluminum foil and a 2 mm large hole was poked into the foil on top of the plates to allow light to enter. Root hair growth was challenged by tilting plates about 20 degree from the vertical plane. Under these growth conditions root hairs grew without surface contact.

2.2.13 Crossing of plants

Using fine-tweezers the anthers of flowers were removed when the petals grew out of the calyx. All remaining older and younger flowers were removed and the prepared flower was fixed on a wooden stick. After one to three days the stigma of the carpels were pollinated with pollen from another plant.

2.2.14 Plant transformation

Plants were transformed according to the “floral dip” method (Clough and Bent 1998). To increase plants fitness they were grown at 18°C until the first flowers appeared on inflorescence. Four days prior to plant transformation a 5 ml pre-culture in YEB medium of the transgenic *Agrobacterium tumefaciens* strain was incubated for two days at 29°C. 1

ml of this pre-culture was used to inoculate the final 200 ml culture, which was incubated for another two days at 29°C. The cells were pelleted at 5800 rpm for 12 minutes. The pellet was resuspended in 5% (w/v) sucrose solution containing 0.05% (v/v) Silwett L-77. Inflorescence were dipped for approximately 20 seconds and afterwards covered with a lid. The lid was removed after two days and after that plants were grown under standard growth conditions.

2.2.15 Seed sterilization

Seeds were incubated for 15 minutes in 3% NaClO₃ (v/v) solution containing 0.1% triton X-100 (v/v). Afterwards they were washed three times with sterile water and then plated on MS-agar-plates (1% Murashige-Skoog salts, 3% sucrose, 0.7% agar-agar, pH5.7, (for screening: kanamycin (50 mg/ml))) (Murashige and Skoog 1962).

2.2.16 Drug treatments

Leaves of wild type (GFP-MAP4 transgenic plants) and *dis2-1* carrying the GFP-MAP4 transgene were dipped in 2.5 µM Oryzalin and visualized at 5 min intervals for a total of 45 min.

2.2.17 Fluorescein diacetate staining

Plant material was incubated for 5 minutes in H₂O containing 100 µg/ml Fluorescein diacetate (FDA). Afterwards the samples were washed with H₂O, mounted on a slide, and analyzed under a spectrophotometric confocal laser scanning microscope (Leica TCS-SP2 AOBS).

2.2.18 Microscopy

Light and epifluorescence microscopy was performed using a LEICA-DMRE microscope using DIC optics (LEICA). Images were taken with a KY-F70 3-CCD JVC camera and frame grabbing DISKUS software (DISKUS, Technisches Büro, Königswinter) was used. Plant measurements were performed with a Leica MZFLIII stereo binocular (LEICA) attached to an Hitachi HVC20 3 CCD camera and frame grabbing DISKUS software (DISKUS, Technisches Büro, Königswinter).

Scanning electron microscopy of *dis2-1* trichomes was carried out as described previously (Mathur *et al.* 1999). For confocal laser scanning microscopy WT and *dis2-1* plants carrying GFP-mTalin and GFP-MAP4 transgenes were grown on MS medium plates as described (Mathur *et al.* 1999), mounted in water and investigated using a 40× water-immersion lens. A spectrophotometric confocal laser scanning microscope (Leica TCS-SP2 AOBS) was used to visualize EGFP (excitation maximum 490/emission maximum 510 nm) as described (Mathur *et al.* 2003a). Images were sized and processed for brightness/contrast and CMYK alterations using the Adobe Photoshop 6.0 software.

2.2.19 Sequence analysis programs

PCR-Primers and constructs were designed using the Vector-NTI-suite 9 software (InforMax, Paisley PA4 9RF United Kingdom). DNA and protein sequence homology searches were performed with the BLAST search algorithm (Altschul *et al.* 1990) from NCBI. Amino-acid sequences were aligned with ClustalW to obtain multiple sequence alignments. Prediction programs were used such as PROSITE, NCBI conserved Domain search and PSORT (ExpASy Proteomics Server).

3 Results

Mutants belonging to the *distorted* class display prominent trichome cell distortions (Hülskamp *et al.* 1994). In this study three genes (*DISTORTED2*, *GNARLED* and *SPIRRIG*) were described and characterized with respect to molecular structure and mutant phenotypes.

3.1 The *DISTORTED2* (*DIS2*) gene

3.1.1 Identification of *DIS2* gene

Three members of the ‘distorted’ class mutants were identified as subunits of the ARP2/3 complex (Mathur *et al.* 2003a, Mathur *et al.* 2003b, Le *et al.* 2003, Li *et al.* 2003). As the ARP2/3 complex in animals consists out of seven subunits, a sequence homology comparison was carried out in which the four remaining ARP2/3 complex subunits were used as templates to identify putative homologs in the *Arabidopsis thaliana* genome. The *A. thaliana* homolog subunits ARPC2 (At1g30825) and ARPC3 (At1g60430) of the ARP2/3 complex are located on chromosome I (Mathur *et al.* 2003a), in the region assigned to *DIS2* (Feenstra 1978). The cDNAs from both genes (At1g60430 and At1g30825) were amplified and subsequently cloned under a cell-specific trichome promoter p*GLABRA2* (Szymanski *et al.* 1998). The *dis2-1* mutant was transformed with these constructs and T1 generation was screened for hygromycin-resistance.

Twenty-five independent hygromycin-resistant *dis2-1* transgenic lines were obtained for each, p*GL2*::At1g60430 cDNA and p*GL2*::At1g30825. They were assayed for complementation of the distorted trichome phenotype. All 25 plants carrying the At1g30825 transgene displayed wild-type trichomes confirming that over expression of this gene in trichomes complemented the effects of the mutation. The T2 progeny of 18 p*GL2*::At1g30825 cDNA transgenic lines showed a 3:1 Mendelian segregation for the

wild-type:mutant trichome phenotype indicating that these lines had a single insertion. No rescue of the trichome phenotype was observed with the At1g60430 cDNA.

In addition, a genomic complementation was achieved by bombarding 8 to 10 days old *dis2* seedlings with 1- μ m gold particles coated with bacterial artificial chromosome (BAC)-DNA (whole BAC t17h7 containing the At1g30825 gene) and p35S::ER:GFP. Wild-type like trichomes expressing GFP were observed between non-GFP-expressing distorted trichomes and confirmed that the BAC containing genomic *DIS2* fragment rescued the trichome phenotype.

These experiments clearly showed that At1g30825 was *DIS2* gene.

3.1.2 Molecular characterization of *DIS2* gene

The primary structure of At1g30825 was evaluated by comparing the cDNA sequence amplified by RT-PCR and the sequence of cloned genomic DNA. The gene consists of 10 exons (Figure 6A) that encode a 957-bp wild-type (Landsberg ecotype) transcript (Figure 6B, wild-type cDNA) and showed conserved AG/GT nucleotides at the exon-intron splice junctions. The sequencing of the At1g30825 gene from *dis2-1* genomic DNA revealed a G \rightarrow A nucleotide exchange at position 1546 in the genomic clone (Figure 6C). This mutation abolished the GT splice donor site at the end of exon 5 and yielded two transcripts of different sizes (Figure 6B, *dis2-1* cDNA): one transcript was 75 bp longer than the wild type due to an extension of exon 5, and the second one was 34 bp shorter than the wild type. In the first case the replacement of the G at the splice donor site by an A created an ATG codon and suppressed splicing. The intron was thus transcribed in continuation of the exon 5 (Figure 6C). The smaller transcript seemed to result from premature splicing that occurred 32 bp upstream of the mutation, at position 1522, where the GT nucleotide combination in exon 5 was apparently recognized as a new donor site (Figure 6D). The sequence alteration generated a new stop codon in both mutant open reading frames (Figure 6C, D, and Figure 7), leading to a non-functional, truncated protein.

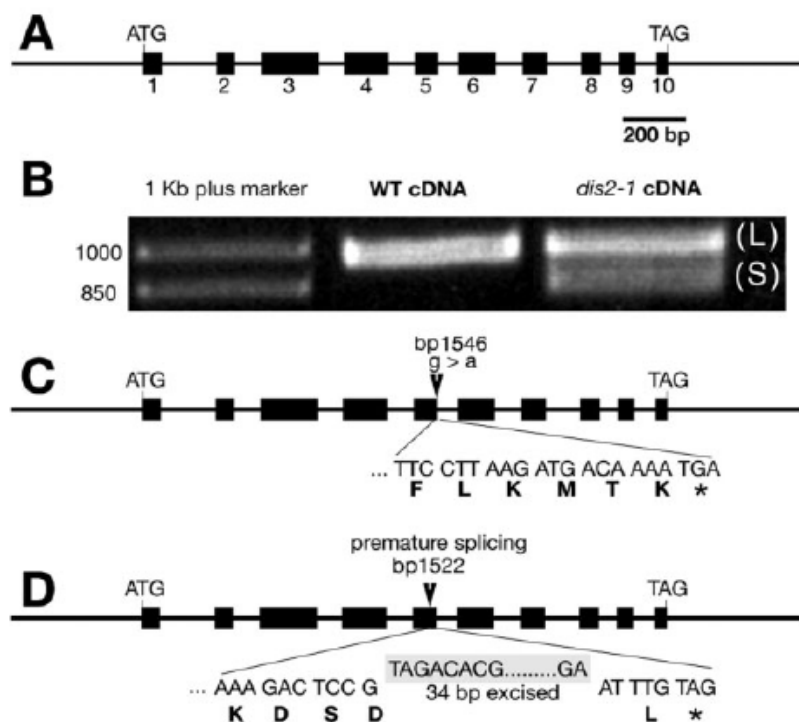


Figure 6. Primary structure of the *DISTORTED2* gene. (A) The *DIS2* (At1g30825) gene contains 10 exons and yields a 957-bp transcript (B). The mutant yields two transcripts; a longer one (L) of 1,032 bp and a shorter one (S) of 923 bp. (C, D) A nucleotide exchange (G → A) at position 1,546 relative to the start codon destroys the GT splice donor site at the end of exon 5. This results in either a longer transcript (6B-L) as a new ATG is created, or generates a premature splice site that is recognized at 1,522 bp (6D) and leads to the excision of 34 bp from the transcript. Both situations lead to premature translational termination.

The 318 amino acid *DIS2* protein featured amino acid identity to the *ARPC2* subunit of the *ARP2/3* complex. Sequence alignment to various animal proteins is shown in Figure 3. BlastP searches in NCBI-database revealed a close plant homolog from *Oryza sativa* (68% identity/ 84% similarity).

Ath	MILLOSHSRFLQILLTACNLD---KAVELDYQWIEFDDVRHVQVTKMKNPNL LLLSVL PNPPEAMSFDGPIGAIHAINITTYGTG-----FQILD	92
Dict	MILLLETHPRTIYDEVI SHFEGDR-----RVNNI FADFDGKFNQ--TSDDKSSLMVSVSLHAAA-----DLLKNGGSSALN SVYGD M-----LQAK	80
Celg	MILLEGNNRTIYELTEQKFA NAKEGGNPE SVNVT FADFDGVLVYKLSNPDGDRTKIILSISLKFYT-----ELQHGADLLRRVYGGH-----MRST	87
Dros	MILLEINNRITIEETLLVKYR NAQAGLNPESIDIRIADFDGVLVYHISNVNGDKTKVRISSISLKFYK-----QLQEHGADLLLRVYG-S-----LITD	86
Hom	MILLEVNNRTIEETLLALKFENAAAGN NPEAVEVTFADFDGVLVYHISNPNNGDKTKVMVSSISLKFYK-----ELQAHGADLLLRVYG-S-----FLVN	86
Rat	MILLEVNNRTIEETLLALKFENAADRN NPEAVEVTFADFDGVLVYHISNPNNGDKTKVMVSSISLKFYK-----ELQAHGADLLLRVYG-S-----FLVN	86
Spom	MISLDYNNRTIYELTEFSSSE-----NPSSIDQVVTDFDGVTFHLS--TPEEKTKLILSLSHKCYE-----ELVNYGTDLNINQIY GAY-----VHE	81
Scer	MLHLQPNLLIQKILNEAIEALRRG-SPLTMDRIVSDFDYTTYVHISNTAEDKSI LLLSVKTKAWVS---VSECQLDGLSLTLNIFLADHYSSLSGGVTIPSE	96
Ath	PRDGSLSLTKLNFSKVRPDE---LLTKLASTREVVMGAFKIIRKHLASRTVAF-----BLDR---LVAIMHRPNETIFLVQADRVIV	171
Dict	PEGGDVITLVIQSSFSGKHE---LAKNVSLLKPRHLVAAPFLMVLEGIEAKKPLP-----EIIA-----INVRIDEITHYLRQGDNIV	156
Celg	PEQGNVITLEYNLADLPADTT---DLVQAASALKRNC FAS---VIEKYFQEQEG-----QEGHKRA-----VINYPDEITHYTEAKDRIV	164
Dros	TEEGYVNSVLIINLEIPEDCI---QIAKRIGLKRNC FAS---VIEKYFYDQEQG-----EEGQKRA-----VINYPDEITLYVEAKPDRIV	163
Hom	PESGYVNSLYLDLENLPASKD---SIVHQAGMLKRNCFAS---VIEKYFQEQEG-----KEGNRA-----VIHYPDEITHYVESKDRIV	163
Rat	PESGYVNSLYLDLENLPASKD---SIVHQAGMLKRNCFAS---VIEKYFQEQEG-----KEGNRA-----VIHYPDEITHYVESKDRIV	163
Spom	PEMGYVNSLIDLQQLPATDKEKQLAMSI SMLKRNVAAPFHRATIKQALADLARKDPENAPMLDKQATS---QELMAIHYRDEEITIVLWBEHDRVIV	178
Scer	VEPGDYITLQITLAEVQES-----ILQSVLKTII LLSFELALSKFIELSQQQ-PAPVEAEITGGVAANGDNTLITIKYRDEENIFIKRSDRIV	189
Ath	AFPMPRFKSDVDTILATSFLEQIVLEARRA-AALNTPASCSTSP-TAPQELGAPKETLSANAG--FVTFVIFPPRHVEGKRLD-PIVNNLSTFHAVVSYHYV	266
Dict	IEDIAFKDADDVILSKIFLQSFVDPRT---ISNVPSITFSQKDPLELEKGVKGVPRAGQANHG--FVSFVIFPPRHKKPQES---ADLIQIFRDVLYHYHYK	249
Celg	IFSTVFKDADDVILGKVFLEFPRGPKA---SQIAPAVLYSLGEPLEIKDLPEARVGNVY--YIIFVIFPPRHINKTKD-MIIDLHSPRDVLYHYHYK	258
Dros	VESTIFRDEDDVILGKVFLEFPRGPKA---SHIAPQVLFSSHREPPLELANT-DARVGNIG--YVIFVIFPPRHINKETRD-MIINLIHSPRDVLYHYHYK	256
Hom	VESTVFKDDDDVILGKVFLEFPRGPKA---SHIAPQVLFSSHREPPLELQDT-DAAVGNIG--YIIFVIFPPRHINASARD-MIINLIHSPRDVLYHYHYK	256
Rat	VESTVFKDDDDVILGKVFLEFPRGPKA---SHIAPQVLFSSHREPPLELQDT-DAAVGNIG--YIIFVIFPPRHINATARD-MIINLIHSPRDVLYHYHYK	256
Spom	VESTVFRDETDRIFGKVFLEFVQARR-PIIQTAPQVLFSTRYDPPLELRDIQGIQKGDFFG--FVIFVIFPPRHFTPNRNE-DCISHIQVPRNTLHSHHYK	274
Scer	IFETIFQDETDRIFGKVFLEFVQARRR-PIIQTAPQVLYSH-EPLELRDILRLYQPPKVAEQSRREHIFVIFPPRHFTQKRIQFHISIQITLFRMYFHYHYK	288
Ath	FSGGMHTMPRREVSMTQALDQAKLEKTR-----SMNNSIKRGLGMEVNHNTNSK	318
Dict	CARGMHTSMRNVESLIIQVLRNRAKPEPVNT-----VKRTITGKFFKQN	293
Celg	CSKAYIHTMPAKTSDFLKVLNRAPEVNG-----EKNITGRTFTQTQ	301
Dros	CSKAYIHTMPAKTSDFLKVLNRAPEPKNT-----EKNITGRTFKRID	301
Hom	CSKAYIHTMPAKTSDFLKVLNRAPEDAEKK-----EMKITGKTFSSR	300
Rat	CSKAYIHTMPAKTSDFLKVLNRAPEDAEKK-----EMKITGKTFSSR	300
Spom	ASKAYMHQMPKRVADFKVLRNRAKPD-----VELERNATGRSFVRA	317
Scer	CSKAYMHSRMPRFVSKFLKVLNRAKVEDDENDELSAEGRQQRRTITGRKIVY	342

Figure 7. The derived amino acid sequence for DISTORTED2 aligned with protein sequences of the ARPC2 subunit of ARP2/3 complexes from reference organisms. (Ath, *A. thaliana* gi-28950897-At1g30825; Dict, *D. discoideum*: gi-10719881; 33% identity, 54% similarity; Celg, *C. elegans* gi-25144430; 28% identity, 48% similarity; Dros, *D. melanogaster* gi-27923962; 26% identity, 48% similarity; Hom, *H. sapiens* AF006085; 26% identity, 46% similarity; Rat, *Rattus* sps gi-27684953; 26% identity, 46% similarity; Spom, *S. pombe* gi-3121760; 26% identity, 46% similarity; Scer, *S. cerevisiae* gi-1730675; 28% identity, 46% similarity). Black areas denote identical amino acids while grey-shaded residues are similar. Asterisks indicate the predicted protein truncation sites in the *dis2*-mutant.

3.1.3 Phenotype of *distorted2-1*

The *distorted2* mutant was first described by its pronounced trichome phenotype (Feenstra 1978) and was found to be a member of the ‘distorted group’ (Hülkamp *et al.* 1994). The *dis2-1* mutant developed leaf epidermal trichomes of irregular shape. Trichome branching occurred but branch lengths were significantly reduced and the branches appeared spike-like compared to wild type. Morphologically these trichomes were stubbed and more swollen (Figure 8). Furthermore, cell alterations were observed in hypocotyl, cotyledon, and root hair cells similar to those observed in *wurm*, *distorted1* and *crooked* mutants (Mathur *et al.* 2003a, Mathur *et al.* 2003b). When grown under low-light conditions, leading to hypocotyl elongation, the hypocotyl length of *dis2-1* mutants was reduced compared to the wild type. The hypocotyl lengths of the mutants were $3.4 \text{ mm} \pm 0.6 \text{ mm}$

and therefore significantly shorter than those of the wild type ($10.3 \text{ mm} \pm 2.2 \text{ mm}$). On the other hand, mutant hypocotyls had increased diameters ($367 \mu\text{m} \pm 61 \mu\text{m}$) in comparison to wild type ($295 \mu\text{m} \pm 29 \mu\text{m}$). These size differences were reflected by alterations on the cellular level: the cells were wider ($40 \mu\text{m} \pm 6 \mu\text{m}$ in the mutant vs. $29 \mu\text{m} \pm 4 \mu\text{m}$ in the wild type) and shorter (ranging from $43 \mu\text{m}$ to $347 \mu\text{m}$ in the mutant and from $340 \mu\text{m}$ to $1154 \mu\text{m}$ in the wild type). Under these conditions the hypocotyl and petiole cells of *dis2-1* de-linked from each other and grew uncoordinatedly under rapid growth conditions as observed for other ARP2/3 mutants (Mathur *et al.* 2003a, Mathur *et al.* 2003b).

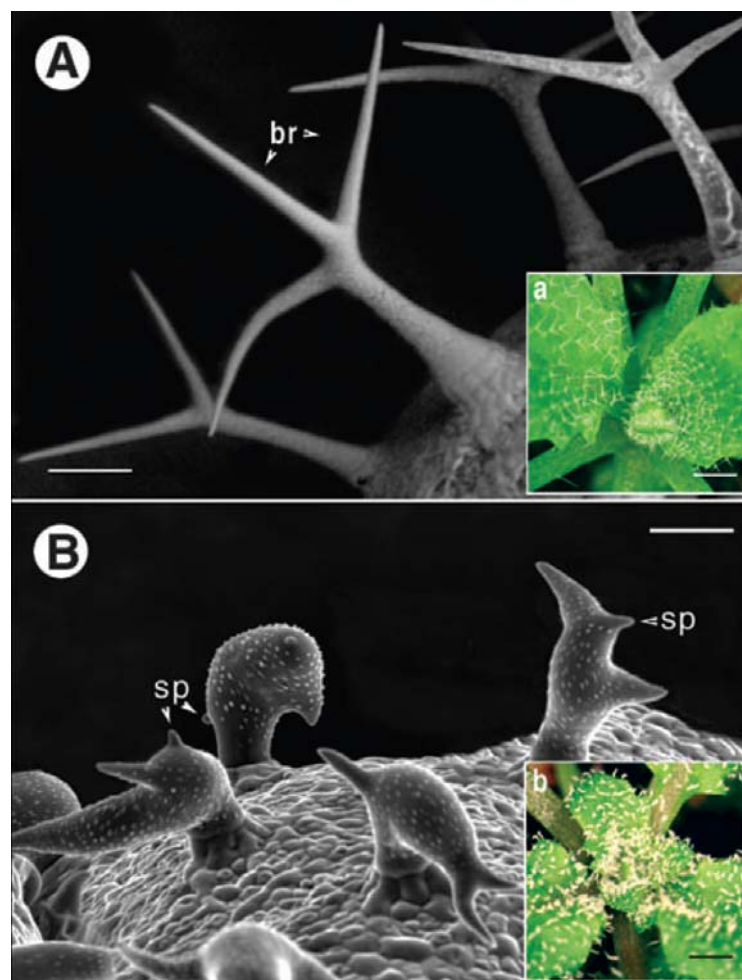


Figure 8. Comparison of leaf trichomes morphology in wild-type *Arabidopsis thaliana* (ecotype Landsberg *erecta*) and *distorted 2-1* mutant. Wild-type trichomes (A) are erect, with well-extended stalks and branches (br). Inset 'a' shows an extended view of trichomes on wild-type leaves. (B) Mutant trichomes are short, randomly distorted and display spike-like (sp) stunted branches. *dis2-1* trichomes (B) are swollen compared to wild-type (A) trichomes. Inset 'b' depicts the distribution of trichomes on mutant leaves. Length standard bars: A, B = $50 \mu\text{m}$; a, b = $250 \mu\text{m}$.

3.1.4 Subcellular phenotype of *dis2-1* mutants

A detailed investigation of the aberrant F-actin cytoskeleton in *dis2-1* mutant trichomes has been published recently (Schwab *et al.* 2003). The description matched the subcellular phenotype described for other ARP2/3 complex mutants (Mathur *et al.* 2003a, Mathur *et al.* 2003b).

The actin cytoskeleton defects accumulated during trichome cell expansion and reached the maximal strength in extending trichome branches of stable p35S::GFP:mTalin transformed *dis2-1* plants. The F-actin, which usually evolved a fine-structure of thin, longitudinally extended cables (as in wild-type trichomes, Figure 9A, B), was typically assembled in short, thick, and cross-linked, bundles (Figure 9C, D). This aberrant F-actin organization increased the number of dense actin patches at the cell cortex (Figure 9C, d), and created local pockets of dense and fine actin (Figure 9D, d). Although dense actin-patches and fine F-actin regions are as well observed in wild-type trichomes at the junction and tips of branches (Mathur *et al.* 2003b), the number of dense actin patches and their location was characteristic in distorted trichomes.

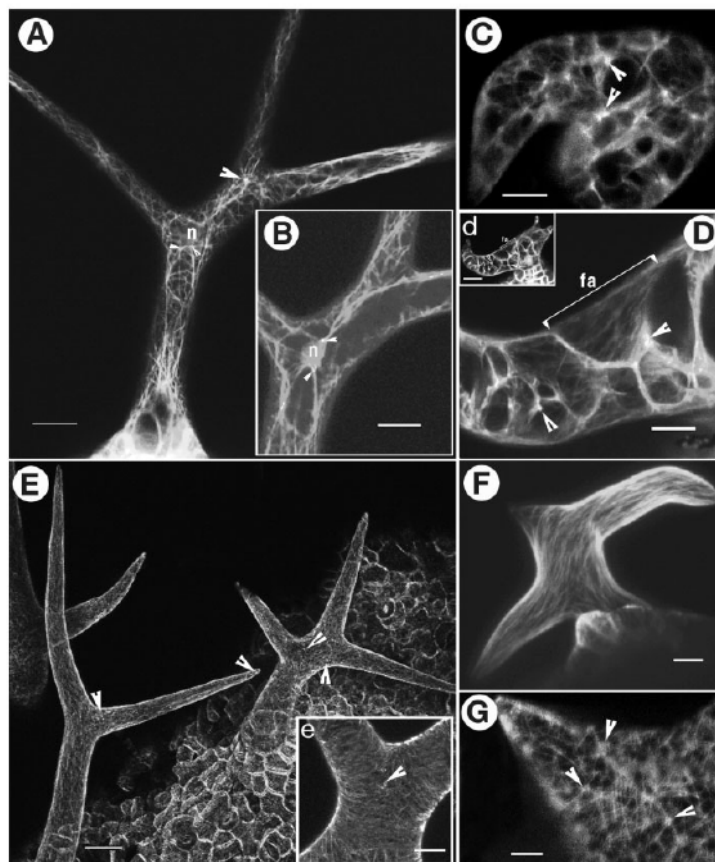


Figure 9 (Page 27). Actin and microtubule organization in *Arabidopsis thaliana* wild-type (Landsberg *erecta*) and mutant trichomes. (A) Cortical actin organization in an expanding wild-type trichome displaying characteristic longitudinally stretched F- (filamentous) actin strands and few actin patches (arrow-heads). (B) A single optical section of trichome in panel A shows actin-patches (arrowheads) in continuity with F-actin strands connecting to the nucleus 'n'. (C) Cortical actin organization in a *dis2-1* trichome at a comparable stage to 'A' displaying more bundled actin filaments and prominent, randomly located actin patches (arrowheads). (D) Portion of *dis2-1* trichome (d) showing local difference in actin organization. Dense actin patches (arrowheads) are interspersed between regions with fine F-actin (fa). (E) The microtubule cytoskeleton in expanding wild-type trichomes. A few dense endoplasmic microtubular foci are observed near branching points and at the tips of branches (arrowheads). (e) Represents a magnified view of the branching region in panel E where microtubule aggregates appear as small bright dots (arrowheads). (F) A stack of five optical sections (1- μm apart) demonstrates that the cortical microtubule organization in a *dis2-1* trichome follows the general contours of the distorted cell. (G) Sections taken between 8 and 16 μm below the outermost optically section, seen in the region of the trichome cell shown in panel F, shows distinct endoplasmic microtubule aggregates (arrowheads). Bars in A, d, E = 20 μm ; B, C, D, F = 10 μm ; e, G = 5 μm . 'n' marks the nucleus. Visualization: actin with GFP-mTalin, microtubules with GFP-MAP₄.

Based on the swollen *dis2-1* trichome phenotype, which is a typical feature of a disrupted microtubule cytoskeleton, an analysis of microtubules in the mutant was performed. Earlier investigations of trichomes from actin drug-treated plants (Mathur and Chua 2000) and different *dis* mutants (Schwab *et al.* 2003) suggested that cortical microtubules maintain their flexibility and usual arrays (wild-type array Figure 9E) despite major alterations in the cell morphology. Consistent with these observations, cortical microtubules followed the general contours of the distorted cell in *dis2-1* trichomes (Figure 9F) and showed that cortical microtubules simply mold themselves to the altered shape. However, in their recent study Schwab *et al.* (2003) focused on cortical microtubules in mature trichomes whereas sub-cortical (endoplasmic) microtubules located 7–15 μm below the outermost optically sectioned layer were not studied. Since endoplasmic microtubules (EMTs) have been shown to play a major role in orientating the growth in *Arabidopsis thaliana* trichomes (Mathur and Chua 2000) the present study used the *GFP-MAP4* fusion construct (Marc *et al.* 1998) to investigate EMT-organization in short, still expanding *dis2-1* trichomes.

In wild-type expanding trichome cells EMTs were prominent at the tubular stage where they preferentially localized to the growing tip; as the cell bifurcates EMTs can be observed at the region of bifurcation and the newly defined tips of branches (Mathur and Chua 2000). With subsequent trichome-stalk and branch expansion EMTs were pushed

against the expanding cell wall by an enlarging central vacuole and it became increasingly difficult to distinguish them from cortical microtubule arrays. EMT clusters usually persisted at the bifurcation point and the sub-apical region in the tips of trichome branches even in mature wild-type trichomes (Figure 9E, e).

Expanding mutant trichomes, however, displayed numerous randomly localized EMT clusters varying in diameter from 3 to 5 μm (Figure 9G). These large inter-connected clusters persisted in mature trichomes giving the microtubule cytoskeleton in *dis2-1* trichomes a general patchy appearance in strong contrast to wild-type trichomes (Figure 9e and 9G).

EMTs have been shown to be more labile than cortical microtubules and they depolymerized readily upon treatment with very low concentrations of microtubule depolymerizing drugs (Sieberer *et al.* 2002). As shown in Table 1, microtubule clusters in *dis2-1* trichomes resisted longer to drug induced de-polymerization than the wild-type trichomes suggesting that they comprise of more stabilized microtubules.

Table 1. Characteristics of endoplasmic microtubule organization in the 6-12 μm region from the outermost surface in expanding ^a wild-type (*Landsberg erecta*) and *distorted 2-1* mutant trichomes.

	wild-type	<i>distorted 2-1</i>
Number of foci	7 \pm 3	45 \pm 18
Position of cluster	Branch point/Branch tip	Random distribution
Size of cluster (x-axis)	2-5 μm	5-12 μm
Drug stability of cluster	10-15 min	35-> 45 min

All observations are based on 25 individual trichomes each from wild-type and mutant.

^a Trichomes without papillate surface decorations on their branches were considered immature and still expanding.

3.2 The *GNARLED (GRL)* gene

3.2.1 Molecular characterization of the *GRL* gene

An initial mapping study discovered the *GRL* gene on chromosome II (Hülskamp *et al.* 1994). A homology search with sequences of the human ARP2/3 subunits against the *Arabidopsis thaliana* genome yielded two homologs of ARPC1a and ARPC1b in the section where *GRL* is located (At2g30910 and At2g31300, respectively). These, however, did not show any sequence differences in *grl* mutants. Therefore neither of the two could represent the *GRL* gene.

However, the phenotypic similarity between *grl* and *arp2/3* mutants suggested that *GRL* and ARP2/3 are components of a common pathway. NAP125 is known to regulate ARP2/3 activity in animals (Eden *et al.* 2002). BlastP search analysis revealed a *NAP125* (At2g35110) *A. thaliana* homolog located on chromosome II where the *GRL* gene had been mapped. The exon-intron structure of the *GRL* candidate gene (Figure 10) was determined by comparing the genomic sequences with cDNA fragments amplified by RT-PCR. This candidate gene featured 22 exons and a 1743 bp long cDNA transcript encoding a putative protein of 581 amino acids.

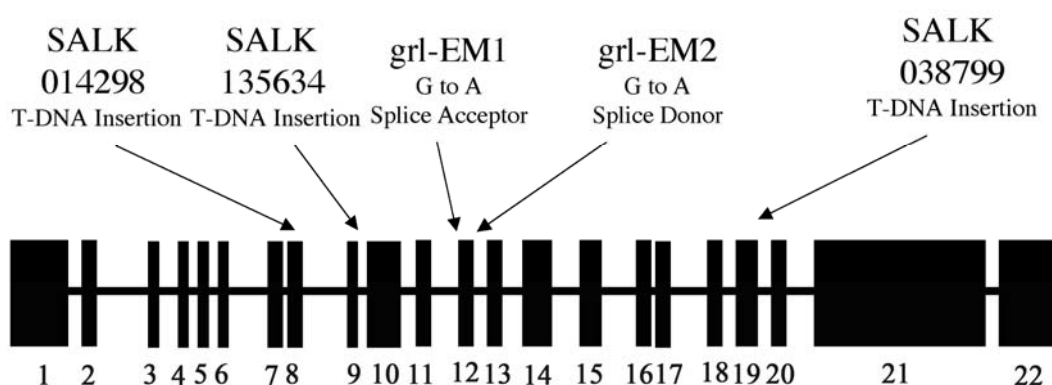


Figure 10. Molecular characteristics of the *GRL* gene. Exon-intron structure of the *GRL* gene as determined by comparison of the genomic DNA with the cDNA sequence amplified by RT-PCR. Exons are indicated as boxes and numbered; introns are indicated by horizontal lines. The positions of the mutations in the different *grl* alleles are indicated.

The assignment of At2g35110 as *GRL* was verified by sequencing various *grl* alleles. The *grl-EM1* showed a G → A nucleotide exchange at the intron-exon splice acceptor site of

exon 12. This mutation was predicted to affect splicing and to yield three altered amino acids followed by a stop codon after 457 amino acids. The *grl-EM2* disclosed a G → A nucleotide exchange at the exon-intron splice donor site of exon 12. Supposedly, this mutation also perturbed splicing and yielded two altered amino acids followed by a stop codon after 493 amino acids. In addition, three T-DNA insertion *grl* alleles (SALK lines 014298, 135634 and 038799) were found carrying insertions in the *GRL* gene (Figure 10). These results clearly showed that the *NAP125* homolog At2g35110 is indeed the *GNARLED* gene.

Protein sequence comparisons revealed similarity to the NAP125 protein from *Drosophila melanogaster* (18% identity, 32% similarity) and NAP125 *Homo sapiens* (17% identity, 32% similarity) (Figure 11). A close homolog of GRL was also found in *Oryza sativa* (66% identity, 72% similarity). Sequences were obtained from NCBI database.

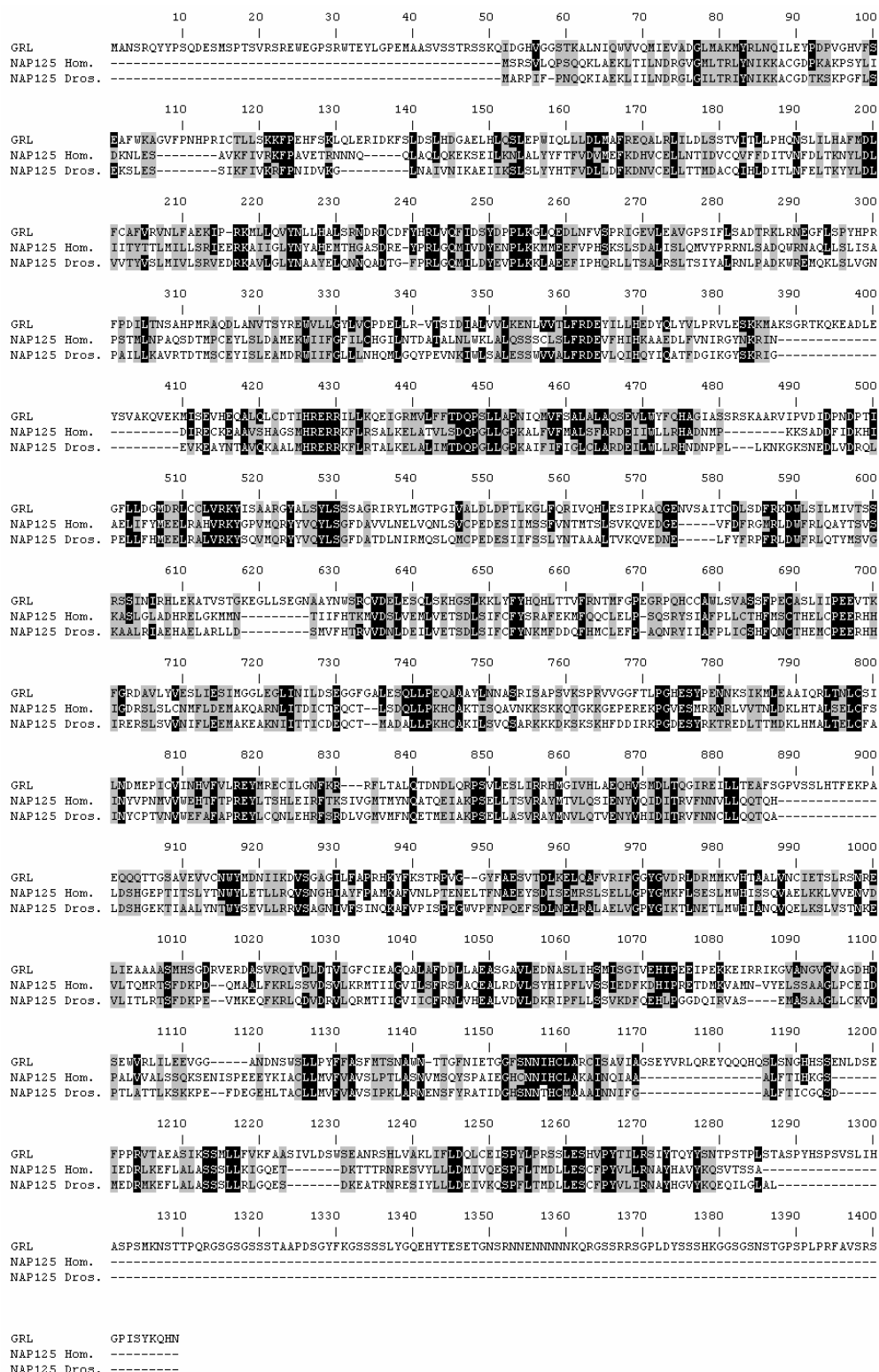


Figure 11. Amino acid sequence comparison of the *Arabidopsis thaliana* GRL gene product with NAP125 from animal species. The sequence of the GRL gene product was aligned with those predicted from NAP125 gene sequences from other species using the ClustalW algorithm (NAP125 Hom., *Homo sapiens* NAP125 Dros., *Drosophila melanogaster*). Identical amino acids are highlighted black; conserved amino acids are indicated by grey shading.

3.2.2 Phenotypic characterization of the *grl* mutants

The trichome phenotype of *grl* mutants was similar to those of mutants defective in genes encoding members of the ARP2/3 complex, like WURM, DISTORTED1, and CROOKED (Hülkamp *et al.* 1994; Le *et al.* 2003; Li *et al.* 2003; Mathur *et al.* 2003a, 2003b). The observation that GRL was not a component of the ARP2/3 complex suggested that like in animals the NAP125 homolog of *Arabidopsis thaliana* controls the activity of the ARP2/3 complex (Figure 12A, B). In order to study whether this regulatory property of GRL was trichome-specific or was also important in other cell types, the mutant phenotypes exhibited by the *grl*-EM1 and *grl*-EM2 alleles were studied in detail.

In all *arp2/3* mutants analyzed so far, the morphology of epidermal pavement cells was severely disturbed (Mathur *et al.* 2003a). While wild-type cells form extensive lobes, structurally comparable to pieces of a jigsaw puzzle, *wrm*, *dis1*, *dis2*, and *crk* mutants have less expanded and less lobed pavement cells (Figure 12C, D). Agarose imprints of the leaf surface were used to analyze the pavement-cell phenotype in *grl* mutants. The *grl* mutants were found to show a similar phenotype to the other *arp2/3* mutants.

The *grl* mutants, like *arp2/3* mutants showed hypocotyl phenotypes compared to wild-type when grown for 8 days under low-light conditions. Hypocotyl wild-type cells expanded rapidly yielding a greatly elongated hypocotyl. However, in *grl* mutants the epidermal cell shape was severely affected. A large number of malformed cells were found, which frequently lost their contacts with other cells and curled outward (Figure 12E, F).

Tip-growing root hairs are not affected in the *arp2/3* mutants, when grown under normal conditions. These mutants, however, form shorter root hairs than wild type once rapid growth is induced by tilting the growth plates 20 degrees downwards from the vertical plane, so the roots have to develop towards the agar. Under these conditions, *grl* mutants also exhibited reduced root hair growth (Figure 12G, H).

In essence, no phenotypic difference could be observed between *grl* and *arp2/3* mutants.

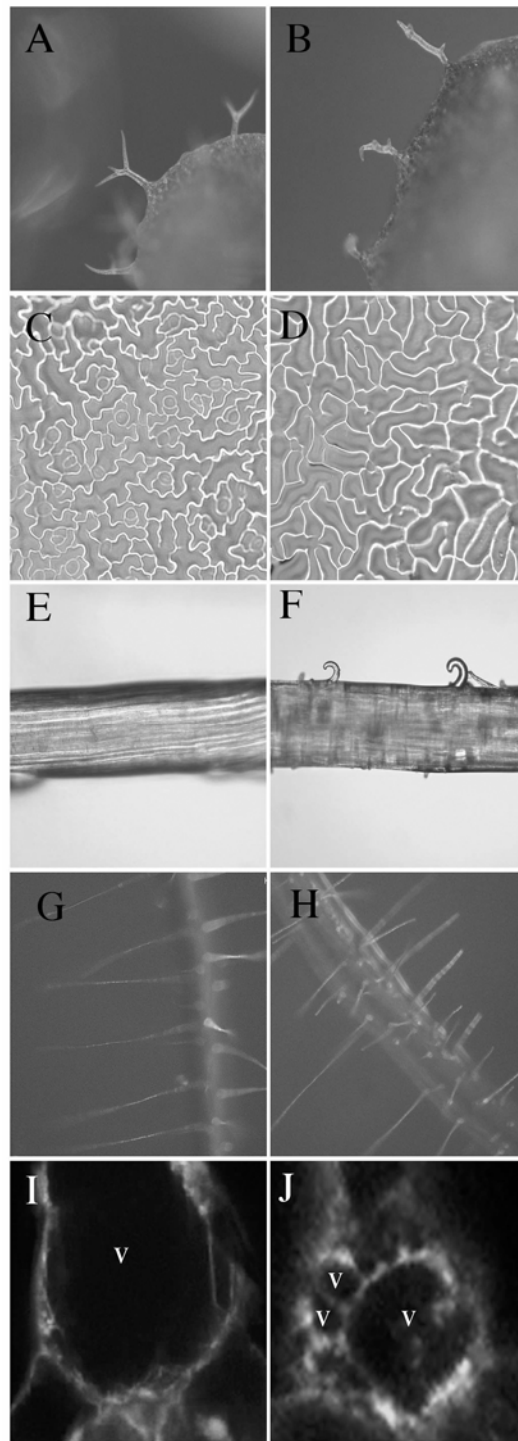


Figure 12. Phenotypic characterization of *grl* mutants. (A) Wild type leaf trichome. (B) *grl* mutant leaf trichomes. Mutant trichomes are randomly shaped and individual branches are either not expanded or more expanded than wild-type trichomes. (C) Wild-type pavement cells adopt a jigsaw puzzle shape due to the formation of lobes. (D) In *grl* mutants pavement cells exhibit a strong reduction in lobe-formation. (E) Low-light-grown wild-type hypocotyl. (F) Lowlight-grown *grl* mutant hypocotyl. The rapid cell expansion caused by growth under low-light conditions yielded shape changes that frequently caused cells to detach from neighboring cells, such that they curl outwards. (G) Wild-type root hairs. (H) *grl* mutant root hairs. Mutant root hairs were generally shorter than in wild type. (I) Fluorescein diacetate (FDA) stained wild-type trichome. The cytoplasm is stained

green, the vacuole is unstained. The wild-type evolved a large central vacuole whereas FDA-stained *grl* mutant trichomes (panel J) demonstrated the formation of extra small vacuoles (V, vacuole).

3.2.3 Subcellular phenotype of *grl* mutants

Actin labeling experiment using GFP-mTalin previously demonstrated that *grl* mutants differed from the *arp2/3* mutants in the organization of the actin cytoskeleton. While *arp2/3* mutants showed a more bundled and patchy actin organization compared to wild type, the *grl* mutant exhibited more “fine actin” (Mathur *et al.* 1999). This phenotypical difference raised the question whether other subcellular changes found in the *arp2/3* mutants could also be detected in the *grl* mutant.

One of the subcellular actin defect phenotypes caused by the application of drugs interfering with actin polymerization was the non existing large central vacuole. Mutants affecting the ARP2/3 complex were also defective in the large central vacuole. Instead, many small vacuoles and vesicles were formed (Mathur *et al.* 2003a). Fluorescein diacetate (FDA), which specifically stained the cytoplasm but not the vacuole (Fricker 2002) due to its dependency on ATP, was used to investigate the organization of the vacuole in the wild type and *grl* mutants. A careful comparison revealed that *grl* mutant trichomes frequently showed small vacuoles separated from the large central vacuole (Figure 12I, J).

3.3 The *SPIRRIG* (*SPI*) gene

3.3.1 The *spirrig* mutant

The *spirrig* (*spi*) mutant was identified during an EMS screen and was grouped into the “distorted class” (Hülkamp *et al.* 1994). The *spirrig* mutant showed a high allele number: *spi-EM1*, *spi-24*, *spi-143*, *spi-174*, *spi-89*, *spi-241*, *spi-273*, *spi-287*, *spi-291*, *spi-296*, *spi-302*, *spi-11*, *spi-4.2*, *spi-12* and *spi-139* (Hülkamp *et al.* 1994, Schwab *et al.* 2003). A rough mapping localized *SPI* on the upper arm of chromosome I, 2.9 cM away from molecular marker *nga59* and 11.48 cM from *nga63* (Schwab *et al.* 2003).

3.3.2 Cloning of the *SPIRRIG* gene

SPI was cloned exploiting positional cloning and gene candidate approaches. For positional cloning a plant of *spi-4.2* allele was crossed to a wild type Col-0 plant and the mapping population was screened in the F2 for *spi* phenotypes and subsequently analyzed with molecular markers. However, the available molecular markers (*nga59* and *nga 63*) for the region of interest on Chromosome I were not sufficient to map the gene precisely. Therefore, new markers were designed based on either simple sequence length polymorphism (SSLP) or derived cleaved amplified polymorphic sequence (dCAPS) techniques. The corresponding data about existing polymorphisms between Col-0 and *Ler* were obtained from the ‘Monsanto *Arabidopsis thaliana* polymorphism and *Ler* sequence collection’. The total mapping population consisted of 502 plants that were screened with different markers. Mapping results are presented in Table 2 and Figure 13.

Table 2. *SPI* mapping. Markers and their description are grouped according to their position on the chromosome I from left to right as indicated in Figure 13.

marker	primer	description	number of recombinant plants	direction
RSM T7I23_1	RS13/RS14	SSLP	13	↓ L
RSM T14P4_2	RS117/RS118	SSLP	4	↓ L
RSM F22D16_1	RS42/RS43	SSLP	0	-
RSM F22D16_2	RS66/RS67	SSLP	0	-
RSM F22D16_3	RS119/RS120	SSLP	0	-
RSM F10O3_2	RS68/RS69	SSLP	0	-
RSM F10O3_3	RS139/RS140	dCAPS	0	-
RSM F10O3_4	RS141/RS142	dCAPS	0	-
RSM F10O3_1	RS15/RS16	SSLP	1	↑ R
RSM F21B7_1	RS40/RS41	SSLP	4	↑ R
RSM F21M11_1	RS38/RS39	SSLP	8	↑ R
RSM T1G11_1	RS36/RS37	SSLP	14	↑ R

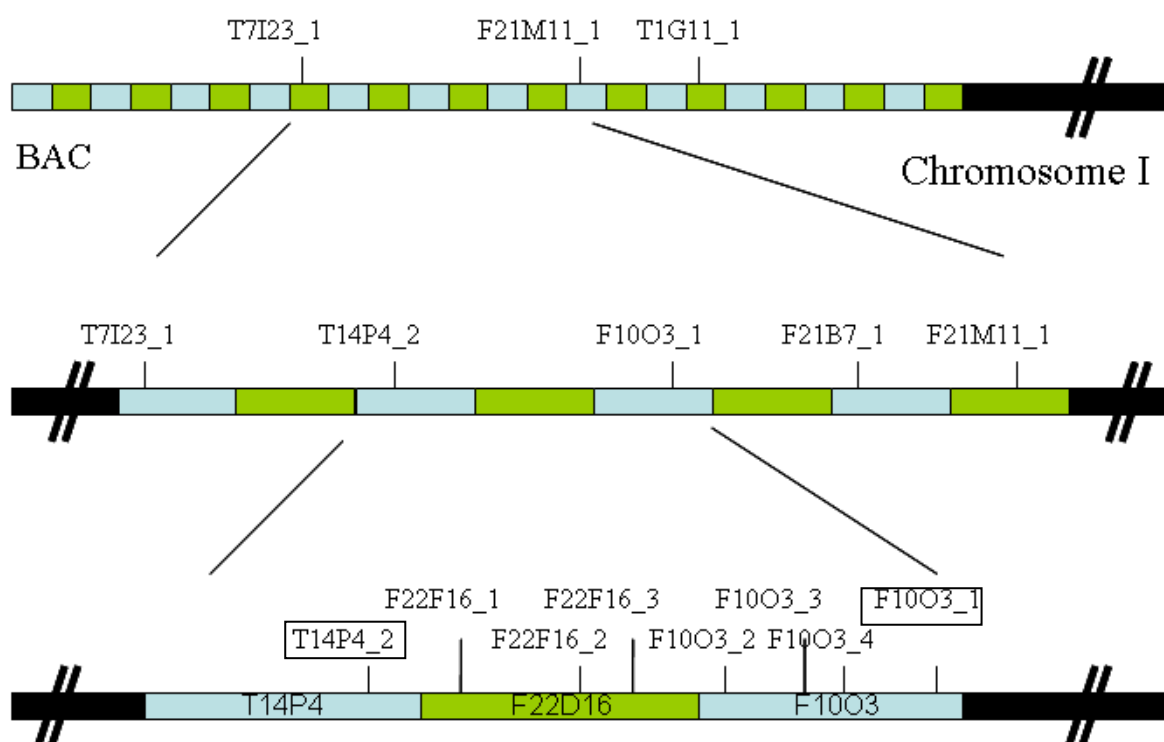


Figure 13. *SPI* mapping flowchart. Schematically drawing of *SPIRRIG* mapping. Upper panel: Bacterial Artificial Chromosomes (BACs) are schematically indicated on the upper end of chromosome I by green and blue boxes. The names and location of the mapping markers are indicated above the chromosome. Panels two and three represent close-ups of panel one.

SPI seemed to be located between markers T14P4_2 and F10O3_1 (highlighted in Figure 13, bottom line). This region, however, was around 120 kb large, and contained 40 characterized, putative, and unknown genes. *SPI* should be located closest to the marker giving the lowest number of recombinants, i.e. F10O3_1 (Table 2).

To further narrow down this 120 Kb region a TILLING (Targeting Induced Local Lesions in Genomes) approach was utilized to detect alterations between the different mutants and the *Ler* background. Unfortunately, the region between marker T14P4_2 and F10O3_1 was very large and the method itself was too inaccurate to achieve coherent results.

Therefore, a gene candidate approach was used instead, based on the allele frequency of *spi* and the assumption that large genes feature higher number of alleles. Within the region close to marker F10O3_1 two candidate genes were determined. The gene prediction yielded large open reading frames (ORFs) for At1g03080 (5232 bp) and At1g03060 (10803 bp). Both gene loci were sequenced in different *spi* alleles and compared to their genomic wild-type sequences. Whereas no mutations were detected in At1g03080, gene At1g03060 exhibited a point mutation in each allele. All analyzed *spi* alleles showed a G → A or C → T exchange, which caused a stop codon in the amino acid sequence suggesting that At1g03060 is the *SPI* gene.

3.3.3 Molecular characterization of *SPI*

Due to the large gene locus (13921 bp) of At1g03060 the isolated cDNA was subdivided into five overlapping pieces. Comparison of the sequences of the genomic DNA and the cDNA stretches revealed that *SPI* mRNA was derived from 19 exons with size ranges between approximately 50 and 1650 bp (Figure 14A). The reconstructed cDNA had a total length of 10803 bp, which could encode a protein of 3600 amino acids.

The mutant allele *spi-11* displayed a G → A alteration 9 bp after the predicted translational start. This mutation created a stop codon after 2 amino acids. In allele *spi-139* a C → T exchange could be detected at the base pair position 3797, causing a stop codon after 705 amino acids. The analysis of the allele *spi-4.2* revealed a G → A exchange at position 10209 on the genomic DNA sequence, which should lead to a stop codon after amino acid 2094. The most distant point mutation was discovered in *spi-12* in which the G → A

exchange occurred at position 13556 bp on genomic DNA. This mutation created a stop codon after 3483 aa. Furthermore a GABI-Kat line was analyzed which revealed a single T-DNA insertion in exon 7 (Figure 14A).

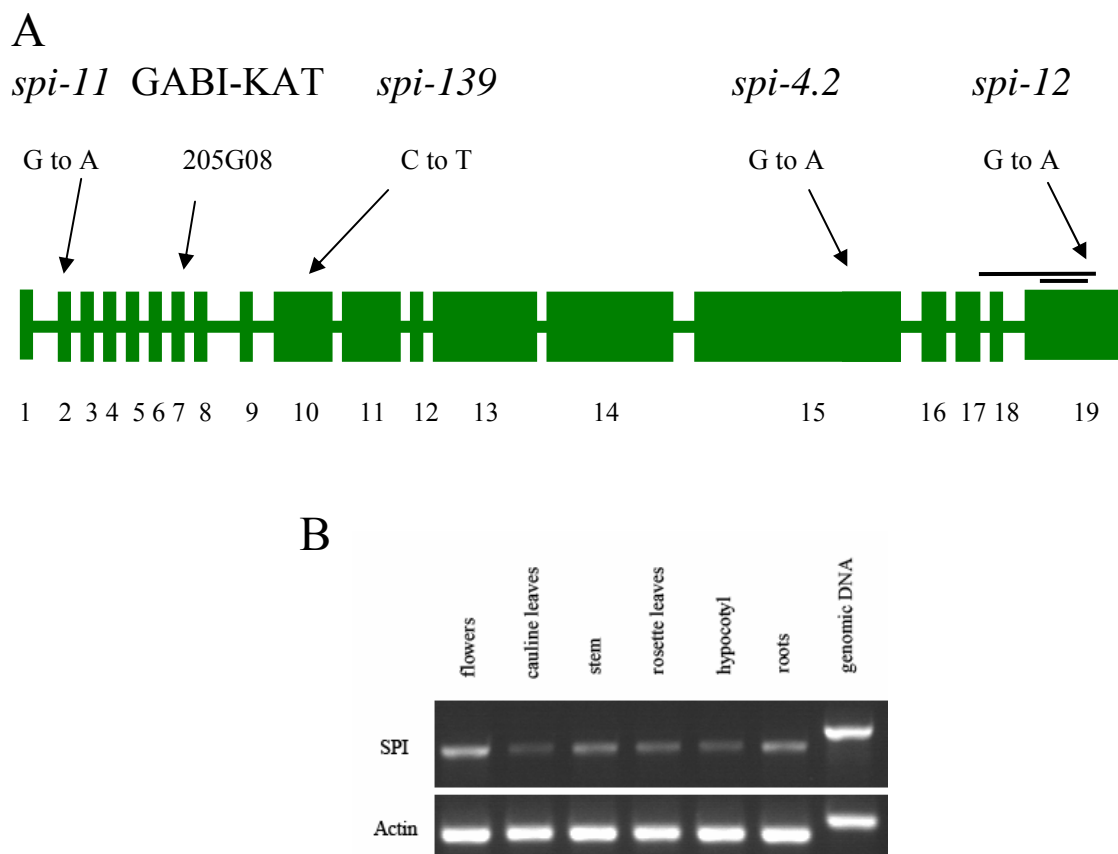


Figure 14. Molecular characterization of the *SPIRRIG* gene. (A) Schematic presentation of the exon-intron structure of the *SPIRRIG*. Exons are shown as boxes and introns as lines. Exons are numbered in black. The positions of point mutations in *spi* alleles are indicated above. The used probes for mRNA detection are indicated as bars above the gene. The small bar indicates probe RS346/RS357 and the large bar indicates probe RS197/RS198. (B) Expression of *SPI* in different tissues as revealed by RT-PCR (30 cycles). A probe (primer RS197/RS198) was used to distinguish between genomic DNA and cDNA (cDNA transcript 1363 bp and 1567 bp on genomic DNA).

The expression pattern of *SPI* was determined by RT-PCR analysis. *SPI* could be amplified from total RNA of all tissues tested including the flowers, cauline leaves, stem, rosette leaves, hypocotyl and roots (Figure 14 B). Ubiquitous *SPI* gene expression was found by using ‘Genevestigator’ (Zimmermann *et al.* 2004) based on an 8.000 unigene containing microarray chip. The analysis of the RNA levels by RT-PCR (30 cycles) revealed no detectable expression in the GABI-Kat insertion allele (Figure 15A), whereas in all EMS-

induced *spi* mutant alleles a transcript could be detected (Figure 15B). All probes used were detecting the 3'-region of the cDNA (Figure 14A).



Figure 15. RT-PCR analysis of different *spirrig* alleles. (A, B) RT-PCR analysis (30 cycles) of *SPI* transcript levels. (A) Wild type and the GABI–Kat insertion allele 205G08 cDNA, detection was based on the larger probe (Figure 14A). (B) Detection of *SPI* cDNA was based on a WD40 domain probe (smaller probe Figure 14A). The WD40 domain probe did not allow detection of differences between cDNA and genomic DNA, but based on the differences in actin, it can be concluded that no genomic DNA contamination is present in the cDNAs of the wild type and the mutants.

According to MIPS database (<http://mips.gsf.de/proj/thal/db/index.html>) annotation the predicted amino acid sequence of At1g03060 exhibits a function in ‘cellular transport, transport facilitation, and transport routes’. The protein consists of 3600 aa with a molecular weight of around 400 kDa and an isoelectric point of 5.75. An investigation of the primary structure of the predicted protein sequence yielded several common motives. PROSITE analysis revealed a ‘Prokaryotic membrane lipoprotein lipid attachment site’ at amino acid 1429 to 1439, an ‘ATP/GTP-binding site motif A (P-loop)’ (2698-2705 aa), a ‘BEACH domain profile’ (2952-3244 aa), and four ‘Trp-Asp (WD40) repeats circular profile’ (3326-3417 aa). A ‘NCBI Conserved Domain Search’ identified the BEACH domain in the same area as PROSITE, whereas slightly different areas were found for the four WD40 repeats (3290-3589 aa) (Figure 16). The BEACH and WD40 domains yielded the highest probability scores. The BEACH domain is described for different eukaryotic proteins and is named after other members of this family, which play a role in the mouse *beige* and the human *Chediak–Higashi* syndrome (Lozanne 2003). A ‘PSORT Prediction’ analysis predicted no N-terminal signal sequence, but seven transmembrane regions (Figure 16) and suggested a Type IIIa membrane protein function with an $N_{\text{cyt}}/C_{\text{exo}}$ membrane topology.

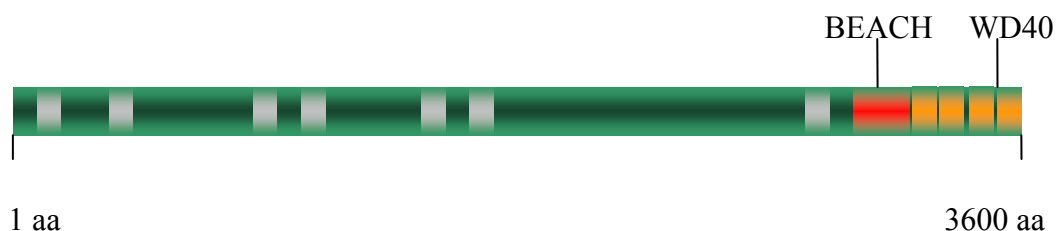


Figure 16. Schematical drawing of the putative SPI protein. The two most important domains detected by domain prediction algorithms are indicated; the BEACH domain is located between amino acid position 2960 – 3244 and WD40 repeat between 3290 – 3590. In grey are the transmembrane domains indicated.

A close *SPI* homolog, At4g02660, which showed 85 % (bl2seq) sequence identity, was detected in the genome of *A. thaliana* by a BlastN algorithm. Screening of four T-DNA insertion lines in At4g02660 obtained from SALK stock center, however, could not be verified and revealed no T-DNA insertion in this particular gene.

3.3.4 Phenotypic characterization of the *spi* mutant

The overall plant size was slightly reduced in all *spi* alleles compared to the corresponding wild-type. This effect was most striking in the *spi-4.2* mutant.

Whereas in most *distorted* mutants the trichome distortion may be very distinctive with a twisted form and increased swelling of the cell producing a bloated distorted cell as observed in *dis2-1* and *grl* trichomes, the phenotype of *spirrig* is more subtle, generating a sinuous form. (Hülskamp *et al.* 1994; Schwab *et al.* 2003) (Figure 17, inset of A-C). Trichome cells in the *spi* mutant are shorter (trichome height $151 \mu\text{m} \pm 22 \mu\text{m}$ compared to $253 \mu\text{m} \pm 22 \mu\text{m}$ for wild-type). Nevertheless, the length/width ratio around 3.5 was almost identical to wild-type with 3.6 (Table 3).

Table 3. Comparison of cellular dimensions of trichomes cells between wild-type *Arabidopsis thaliana* (ecotype-Landsberg *erecta*), and *distorted2* (*dis2*), *crooked* (*crk*), and *spirrig* (*spi*) mutants. Trichome stalks were measured between the support cells and the first branch point/short branch initial; Branch length (all μm) was measured from its origin at the stalk to its tip; Trichome height is given as the distance between the base of the stalk and the highest extended branch. Average value \pm standard deviation is based on 75 counts each.

	stalk length	stalk width	ratio l/w	branch length	trichome height
wt	111 \pm 16	31 \pm 4	3,6	149 \pm 23	253 \pm 22
<i>dis2</i>	41 \pm 10	33 \pm 5	1,1	70 \pm 13	114 \pm 16
<i>crk</i>	41 \pm 9	28 \pm 4	1,4	53 \pm 20	113 \pm 16
<i>spi</i>	66 \pm 10	19 \pm 4	3,5	94 \pm 24	151 \pm 22

Three branches were initiated and extended up to 94 $\mu\text{m} \pm 24 \mu\text{m}$ compared to a branch length $> 150 \mu\text{m}$ for wild-type trichomes. In most of the *spi* trichomes, the distance between the first and the second branching point was larger than in the wild type. Compared to the trichomes of the *crk* or *dis2-1* mutant the overall dimensions of the *spirrig* mutant were closer to wild-type values (Table 3). The *spi* mutant had no reduction of branch point numbers; this is a common feature of all *distorted* mutants.

Further shape aberrations were described for other cell types like pavement, hypocotyls, and root hair cells in the phenotypical characterization of *distorted1*, *wurm* and *crooked* mutants by Mathur *et al.* (2003a, 2003b) and for *grl* and *dis2-1* in this study. The *spi* mutant alleles displayed similar defects in these cell types (Figure 17).

The complexity of epidermal pavement cells, given as the ratio between perimeter and area using the formula: $\text{perimeter}^2 / (4 \times \pi \times \text{area})$ (Dewitte *et al.* 2003), revealed a significant ($p \leq 0.01$) reduction of lobes in the EMS mutants compared to wild-type (Figure 17 and Table 4). However, no difference could be observed between the T-DNA line 205G08 and the corresponding COL-0 wild type.

Some hypocotyl cells in the *spi* mutant at the hypocotyl surface and petioles of cotyledons were disconnected from each other and curled out of the epidermal plane along the longitudinal growth axis (Figure 17). Furthermore, the overall hypocotyl length of *spi* plants was significantly ($p \leq 0.01$) reduced 8 days after germination (DAG) compared to wild-type. Both effects were equally strong in all investigated *spi* alleles. These growth deficiencies and detachment of cells were observed when plants were grown under low-light conditions. Similar effects with different significance were reported for other ARP2/3 mutants as well (Mathur *et al.* 2003a, 2003b).

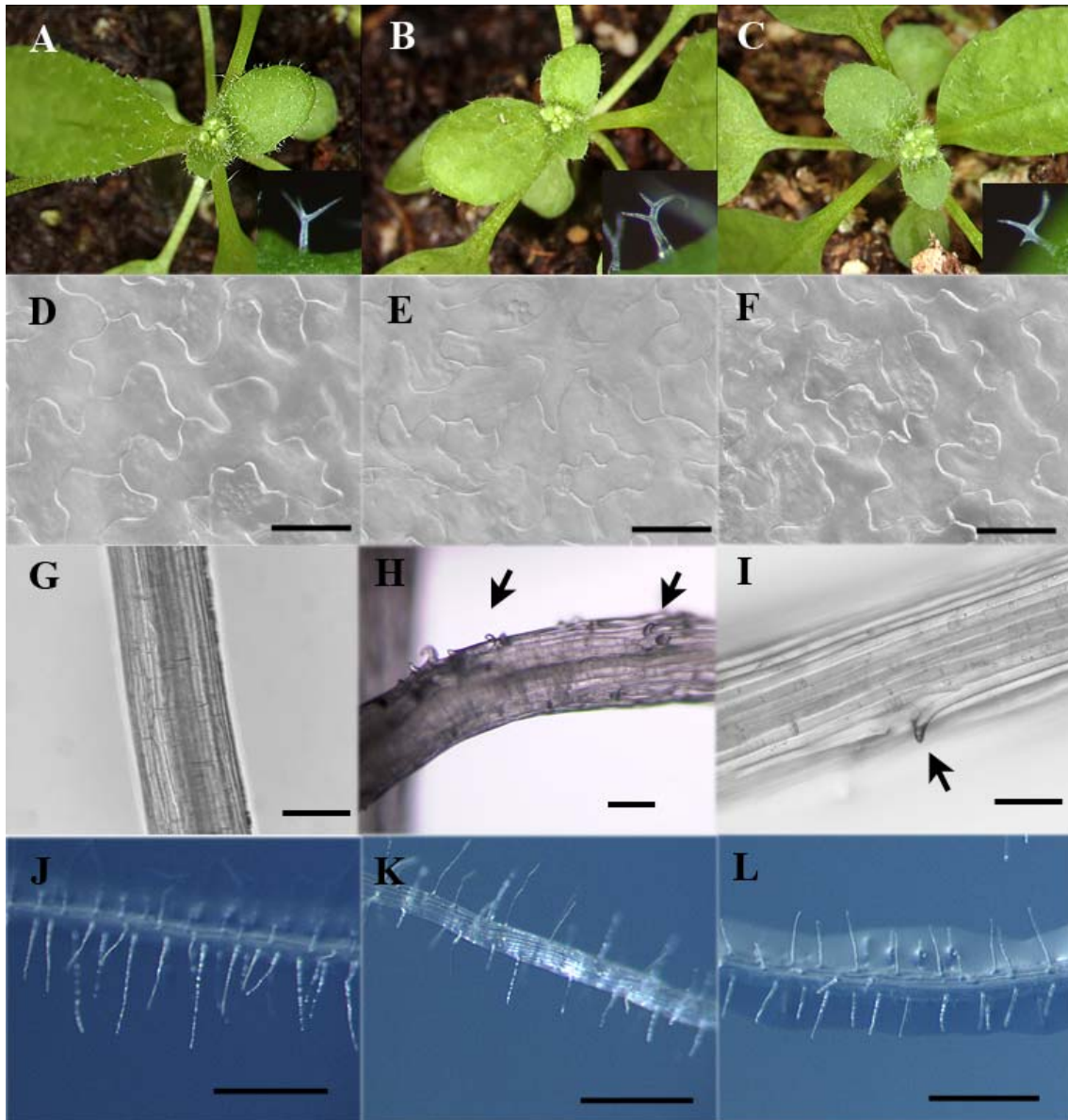


Figure 17. Phenotypic characterization of *spi* mutants. As examples, a mutant with an early and a late stop codon mutation. (A-C) Rosette plants; inset shows trichomes. (A) Wild type. (B) *spi-11* mutant. (C) *spi-12* mutant. (D-F) epidermal pavement cells. (D) Wild-type. (E) *spi-11* mutant. (F) *spi-12* mutant. (G-I) Hypocotyl of low-light-grown plants (G) wild-type. (H) *spi-11* mutant. (I) *spi-12* mutant. The rapid cell expansion caused by growth under low-light conditions yielded shape changes that frequently caused cells to detach from neighboring cells, such that they curl outwards. Arrows indicate those cells in H-I. (J-L) root hair cells (J) Wild-type. (K) *spi-11* mutant. (L) *spi-12* mutant. Mutant root hairs were shorter than in wild type. Bars in D-F = 50 μm ; G-I = 200 μm ; J-L = 500 μm .

After 8 DAG the root hair cells in *spi* were, when exposed to rapid growth, dramatically reduced in size in all *spi* alleles in comparison to the wild-type ($p \leq 0.01$) (Figure 17 and Table 4). The reduction in size was stronger in *spi* than in *dis2* or *grl* mutant alleles.

Table 4. Comparison of cellular dimensions between wild-type and *spirrig* (*spi*) mutants in the complexity of pavement cells, hypocotyl (mm) and root hair length (μm). Average value \pm standard deviation is based on 50 counts each.

	complexity of pavement cells	hypocotyl in [mm]	root hair in [μm]
Ler wild type	5.4 \pm 1.8	11.0 \pm 1.9	547 \pm 137
<i>spi-11</i>	3.6 \pm 0.9	6.0 \pm 1.5	180 \pm 50
<i>spi-139</i>	2.9 \pm 0.7	6.1 \pm 1.2	198 \pm 95
<i>spi-4.2</i>	4.2 \pm 1.6	5.0 \pm 1.6	172 \pm 68
<i>spi-12</i>	3.3 \pm 1.0	6.6 \pm 1.2	207 \pm 43
Col wild type	3.5 \pm 1.2	12.9 \pm 2.4	550 \pm 120
205G08	3.8 \pm 1.3	6.6 \pm 0.9	112 \pm 37

3.3.5 Subcellular phenotype of *spi* mutants

The F-actin cytoskeleton was investigated by crossing the GFP-mTalin construct into the *spi-4.2* allele. Analysis under the confocal microscope revealed that the actin cytoskeleton was not altered when compared to wild type (Schwab *et al.* 2003). The F-actin strands were structured into fine, longitudinally extended cables located at the cortical area of the cell that were oriented towards the tips of the branches. The inner area of the cell was entirely occupied by the central vacuole. These observations differ from the *dis2-1* and the *grl* mutant, in which the actin cytoskeleton was completely disturbed.

4 Discussion

Arabidopsis thaliana leaf epidermal trichomes represent a perfect assay system to study cell morphology due to the predictability of their mature cell shape. Trichome cells, whether branched or unbranched, are connected at their base only to socket cells of epidermal tissue, while their major parts are freely protruding from the leaf surface. Therefore, the impact of other cells is marginal and any alteration in cell growth is directly reflected in their cell shape, which is easy to recognize. A group of cell shape mutants was described as *distorted* mutants (Hülkamp *et al.* 1994), most of them revealed a disorganized actin cytoskeleton (Mathur *et al.* 1999, Szymanski *et al.* 1999), except one member, namely *spirrig* (Schwab *et al.* 2003).

The three genes studied herein encode representative proteins of three different complexes affecting cell shape:

- DIS2, a component of the ARP2/3 complex,
- GRL, a component of the PIR121/NAP125/Abi2 complex, and
- SPI, a novel component related to BEACH/WD40 domain proteins.

4.1 DISTORTED2, a component of the ARP2/3 complex

As described before, the ARP2/3 complex is a component of the actin cytoskeleton and in animals is composed of seven subunits. Three genes belonging to the *DISTORTED* class have already been identified as subunits of the ARP2/3 complex based on protein homology (Mathur *et al.* 2003a, Mathur *et al.* 2003b, Le *et al.* 2003, Li *et al.* 2003). The results presented herein identified DISTORTED2 (DSI2) as the fourth component of the ARP2/3 complex.

Molecular analysis including complementation of the mutant revealed that At1g30825 is *DIS2*, which contains 10 exons and encodes a protein of 318 amino acids. *DIS2* features homology to *ARPC2* and could be part of the ARP2/3 complex based on this criterion. Complementation of *Arabidopsis thaliana* mutants with respective animal homologs (Mathur *et al.* 2003b) and the rescue of yeast mutants by plant homologs (Le *et al.* 2003, El-Din El-Assal *et al.* 2004) suggest a high degree of functional conservation of the ARP2/3 complex.

Given this functional conservation, one would expect that in plants the ARP2/3 complex also consists out of seven subunits. However, the fact that only four subunits have been identified as part of this complex so far and since there are no further unassigned *distorted* mutants known, except *alien*, there could be at least three more proteins involved in ARP2/3 complex formation that remain unidentified. One explanation for this could be that the plant ARP2/3 complex may have fewer subunits than the known complexes from other organisms. On the other hand, there might be also a high redundancy of ARP2/3 subunits in planta. Biochemical isolation and analysis of the complex might clarify this situation.

4.1.1 The *distorted2* mutant phenotype

Although the molecular basis of the actin cytoskeleton changes in three, *crk*, *dis1*, and *wrm* previously characterized ARP2/3 mutants were exhaustively investigated, the results did not explain the distorted trichome phenotype sufficiently. This phenotype apparently emerges from random localized changes in growth directionality. Changes in growth directionality, however, are usually associated with alterations in the microtubule cytoskeleton (Bibikova *et al.* 1999, Mathur and Chua 2000, Mathur and Hülkamp 2002, Ketelaar *et al.* 2003). The finding that the microtubule cytoskeleton is also aberrant in the *dis2-1* mutant implies major significance and promotes the discussion of the causes for polar growth directionality fixation in plant cell.

4.1.2 Localized growth

The growth of a plant cell in a particular direction reflects ‘molecular decisions’ made inside the cell. The deposition of external cell-wall building components and the typical

alignment of cellulose microfibrils are thus manifestations of internal processes. This may explain why, despite well-documented observations that microtubules are involved in establishing and maintaining growth directionality in plant cells (Bibikova *et al.* 1999, Mathur and Chua 2000, Mathur and Hülskamp 2002), an earlier study (Schwab *et al.* 2003) that reported normal configurations of cortical microtubule arrays in distorted trichomes, could not conceive of a convincing role for microtubule involvement in cell shape distortion.

The endoplasmic microtubule organization is considerably altered in *dis2-1* mutants, as shown in this study, even though the array of cortical microtubules appears normal (Figure 9). This is also underlined by the fact that the actin inhibiting drug latrunculin-B (lat-b) altered the endoplasmic microtubules (EMT) (Saedler *et al.* 2004a). EMTs, that are known to be very labile and active in living cells, are explicitly involved in polarized growth (Bibikova *et al.* 1999, Mathur and Chua 2000, Sieberer *et al.* 2002, Ketelaar *et al.* 2003). However, the molecular mechanism how EMTs are directed towards specific cortical locations and how they perform their functions in determining directions and fixing polarity during polarized growth of plant cells remains unclear.

Contextual studies in other organisms have clearly shown that cytoplasmic microtubules search for cortically located cues defined by the actin cytoskeleton (Hayles and Nurse 2001, Rodriguez *et al.* 2003). The fact that, like in other *arp2/3* mutants, the *dis2-1* mutant shows cell shape defects, based on alterations in actin and microtubule cytoskeleton, may suggest that a similar mechanism operates in higher plant cells as well.

4.1.3 Cortical actin mesh

Studies on different cells have shown that the earliest indication for a change in growth directionality inside a cell is the appearance of a small bulge on the cell surface (Baluska *et al.* 2000, Mathur and Chua 2000). The bulge emerges from a localized weakening of the cell cortex (Baluska *et al.* 2000). This process has been experimentally invoked through drug-induced destabilization of the actin cytoskeleton (Ketelaar *et al.* 2003). A similar requirement for dynamic cortical actin has also been reported for polarization and rhizoid-pole establishment in fucoid zygotes (Alessa and Kropf 1999, Hable *et al.* 2003). Another link between fine F-actin formation and cell morphology is suggested by observations of

atypically swollen cells in transgenic plants overexpressing a constitutively active form of AtROP2 (Fu *et al.* 2002). The discussion of the *crooked* phenotype has proposed that loosening of the actin mesh that delineates a cellular site for localized growth is accomplished *in vivo* by ARP2/3 complex-mediated increase in actin polymerizing activity (Mathur *et al.* 2003b). Depending on the F-actin mesh size the cortical F-actin may furthermore act as a barrier for the movement of vesicles as well as for the targeted deposition of growth materials. However, the actin mesh-based model did neither elaborate how a weakening of the actin mesh, once initiated, could be directed to produce local expansion, nor did it explain how the directionality of this expansion could be maintained in a growing cell. The observations on *dis2-1* now allow a more detailed view on these mechanisms.

4.1.4 Possible interaction of cortical actin and microtubules

A broadened weakening over a large area of the cell cortex would allow the growth process to spread over a larger area through non-targeted delivery of growth material by vesicles and thus expand the cells globally.

However, if cortical weakening could be controlled and limited to a small region of the cell, growth processes would take place in this region. Since the actin cytoskeleton, implicated in the weakening process, may be unable to restrict its own activity, another fibrous, rapidly polymerizing cytoskeletal component may be required at the weakened site. Based on endoplasmic microtubules disruption in the *dis2-1* mutant these endoplasmic microtubules represent strong candidates for the function that carry out these vital responses by establishing a ‘reinforcing patch’ around the impairment site. A recent observation involving the microtubule plus-end-binding protein AtEB1b (Mathur *et al.* 2003c) suggested that growing microtubule ends can reconfigure endo-membranes.

The fact that loss of microtubule activity invariably leads to non-polarized, isotropically expanding cells strongly supports the microtubule involvement in regional growth restriction (Mathur and Chua 2000, Mathur and Hülskamp 2002). Moreover, observations on tip growing root hairs and pollen tubes have revealed that microtubules are absent from the apolar bulge that is produced in cells prior to their embarking on polarized growth (Baluska *et al.* 2000, Carol and Dolan 2002). Their subsequent appearance in the bulged domain usually determines the growth directionality and leads to true polarized growth

(Baluska *et al.* 2000, Carol and Dolan 2002). Polar growth fixation obviously requires microtubules present at a cortical site that has been impaired due to alterations in actin organization.

4.1.5 Cell growth

Based on the molecular lesions the primary cytoskeletal defect in *crk*, *dis1*, *dis2*, and *wrm* trichomes was their cortical actin organization. Wild-type trichomes exhibit maximal actin aggregation near trichome branching points and the tips of branches (Mathur *et al.* 2003b) whereas actin aggregates excessively in random locations in the mutant trichomes. The same regions where actin aggregation is seen in wild-type trichomes are also areas where asters like more stable microtubule formations have been described in wild-type trichomes (Mathur and Chua 2000). Moreover, a transient stabilization of endoplasmic microtubules is sufficient to alter growth directionality in expanding trichomes (Mathur and Chua 2000). The coincidence of the localization of actin patches and microtubule foci in cellular proximity (Saedler *et al.* 2004a) and the growth directionality changes in the mutants suggests an intimate spatio-temporal cooperation and interdependence between the actin and microtubule cytoskeleton.

Studies on other plant cell types using immunocytochemical methods have also observed local proximity between actin and microtubule elements (Collings and Allen 2000 and references therein). The random localization of cortical actin patches in *distorted* mutants described so far and the assignment with the *dis2-1* mutant seem to relate the placement of endoplasmic microtubules. These sites of coincident localization may therefore represent sites of altered growth directionality in the cells (Figure 18). This leads to a model in which the local increase of cortical actin dynamics (loose mesh) serves as a starting point for polarized growth. This polar growth directionality is established by endoplasmic microtubules and then all growth-related intracellular traffic is diverted to the specific site (Mathur 2004). This model is supported by an interesting finding namely that in budding yeast the ARPC2 subunit (a homolog of DIS2) is involved in two genetically distinct calmodulin-mediated functions that independently regulate the actin and microtubule cytoskeleton (Schaerer-Brodbeck and Riezman 2000).

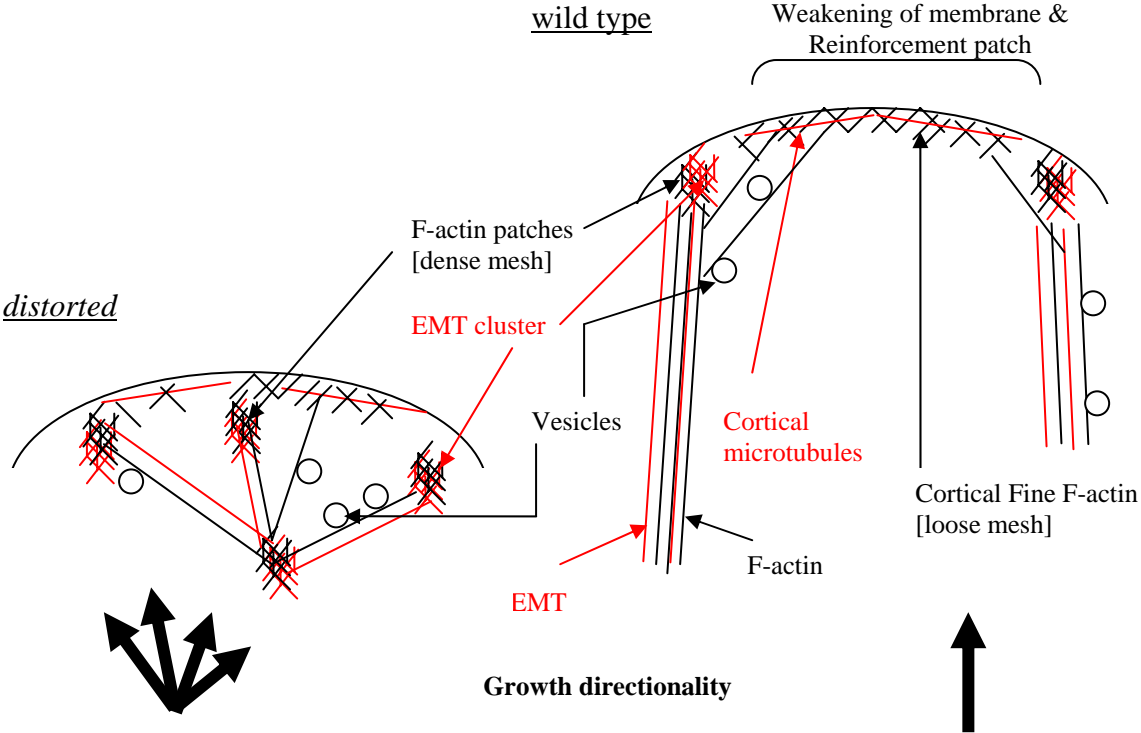


Figure 18. Schematical drawing of a view through a cell. Left: random distribution of actin patches and microtubule clusters in the *distorted* mutants, leading to a random growth with random growth directionality. Right: the wild type situation, leading to one growth directionality, in which EMT restrict the local growth site.

The increased number of growth sites in *distorted* mutant trichomes compared to wild-type trichomes strongly suggests that such localized growth changes occur repeatedly during mutant trichome development. The cumulative changes could yield a randomly distorted trichome cell as observed in this study. In contrast, the fixation and therefore restriction of growth sites (Figure 18) would result in the typical wild-type shaped trichome cell. The connection shown between the actin and microtubule cytoskeleton in the *dis2-1* mutant might hence give insight how complexity of plant cells could be generated.

4.2 GNARLED, a potential regulator of the ARP2/3 complex

The molecular and cell biological analysis of the ‘distorted group’ of trichome mutants displaying randomized expansion has greatly improved the understanding of actin-based cellular growth processes (Mathur and Hülskamp 2002, Deeks and Hussey 2003, Smith 2003). The common mutant trichome phenotype and the relation of strong mutants *crk*, *dis1*, *dis2*, *wrm*, *grl*, *klk* and *ali* with actin defects suggest that all of these seven genes are involved in the regulation of the actin cytoskeleton (Hülskamp *et al.* 1994, Mathur *et al.* 1999, Szymanski *et al.* 1999, Le *et al.* 2003, Li *et al.* 2003, Mathur *et al.* 2003a, 2003b, Schwab *et al.* 2003, El-Din El-Assal *et al.* 2004, this study: Saedler *et al.* 2004a). Four of these genes (*CRK*, *DIS1*, *DIS2* and *WRM*) encode components of the ARP2/3 complex, which is known to modulate actin organization at sites of active growth (Li *et al.* 2003, Mathur *et al.* 2003a, 2003b, El-Din El-Assal *et al.* 2004, Le *et al.* 2003, this study: Saedler *et al.* 2004a). Since the mutants affected in the *GRL* gene share all the phenotypic features found in *arp2/3* mutants, it was obvious to investigate whether *GRL* was part of the ARP2/3 complex or its regulatory pathways.

In animals the ARP2/3 complex is regulated by two independent pathways, the WASP and WAVE/SCAR pathway (Figure 5). Homology searches revealed that plants lack homologs of WASP, which suggests that this regulatory pathway is absent in plants (Deeks and Hussey 2003). In contrast, the existence of a WAVE/SCAR-related regulation pathway in plants was suggested by the identification of several components (Deeks and Hussey 2003). In this pathway the most known upstream regulators so called ROP proteins (Rho’s of plants) were identified in plants, and some of them were shown to be involved in actin-dependent cell growth processes (Mathur and Hülskamp 2002b, Yang 2002). In addition, BRICK1, an HSPC300 homolog in maize has been shown to be involved in actin-driven lobe formation by epidermal pavement cells (Frank and Smith 2002) (Figure 19; Table 5). The cloning and characterization of *GRL* as the homolog of NAP125 shows that one member of the ternary complex (PIR121/NAP125/Abi2) exists in plants. However, sequence identity of *GRL* to known members of NAP125 is fairly low, but the rescue of the plant mutant phenotype by the human NAP125 gene proved its functional conservation (El-Assal *et al.* 2004). This conclusion was supported by other groups which published a

characterization of this particular gene independently (Deeks *et al.* 2004, El-Assal *et al.* 2004, Brembu *et al.* 2004, Li *et al.* 2004).

Table 5. Comparison of some molecular animal actin-pathway players to their counterparts in plants.

Animal protein/complex	Plant protein/complex
Rho family GTPases	11 Rho-like proteins of plants (ROP) in <i>Arabidopsis</i> (Vernoud <i>et al.</i> 2003); putative ROP- guanine nucleotide exchange factor (GEF) (Qiu <i>et al.</i> 2002); multiple GTPase-activating protein (GAP), guanine nucleotide dissociation inhibitor (GDI), and novel ROP effectors (Gu <i>et al.</i> 2004)
WAVE/SCAR	SCAR-related in <i>Arabidopsis</i> (Frank <i>et al.</i> 2004); DISTORTED3 (Basu <i>et al.</i> 2005)
NAP125	GNARLED (Deeks <i>et al.</i> 2004, El-Assal <i>et al.</i> 2004, Brembu <i>et al.</i> 2004, Li <i>et al.</i> 2004, Zimmermann <i>et al.</i> 2004)
PIR121	KLUNKER (Basu <i>et al.</i> 2004, Brembu <i>et al.</i> 2004, Saedler <i>et al.</i> 2004b, Li <i>et al.</i> 2004)
HSPC300	BRICK1 (Frank and Smith 2002)
Abi-1	Four predicted proteins in <i>Arabidopsis</i> (Deeks <i>et al.</i> 2004); ABIL-1 (Basu <i>et al.</i> 2005)
ARP2/3 complex	Four subunit homologues present (Li <i>et al.</i> 2003, Mathur <i>et al.</i> 2003a, 2003b, El-Din El-Assal <i>et al.</i> 2004, Le <i>et al.</i> 2003, Saedler <i>et al.</i> 2004a)
Formin(s)	Numerous formin-like (Deeks <i>et al.</i> 2002, Ingouff <i>et al.</i> 2005)

Out of the ternary complex another member, namely PIR121 was independently identified from different groups (Basu *et al.* 2004, Brembu *et al.* 2004, Saedler *et al.* 2004b, Li *et al.* 2004). The *KLK* gene (one member of the *DISTORTED* genes) was found to be identical to PIR121. The PIR121 and its human homolog bind interchangeably and with a high degree of specificity to active forms of the human RAC1 and the plant counterpart ROP2 small GTPases (Basu *et al.* 2004). The two members, GRL and KLK were shown to interact with each other and with their human homologs (El-Assal *et al.* 2004) (Figure 19).

Another recent discovery was the identifications of three WAVE/SCAR activator proteins in *Arabidopsis thaliana*. Whereas some full-length WAVE/SCAR proteins bound *in vitro* with an *Arabidopsis thaliana* homolog of HSPC300 (AtBRICK1) and therefore suggested an interaction *in vivo* to regulate the ARP2/3 complex (Frank *et al.* 2004). For another WAVE/SCAR protein (DISTORTED3) it was reported to interact with an ABI1-like bridging protein from *Arabidopsis thaliana* (Basu *et al.* 2005). Four ABI proteins were beforehand predicted to exist in the *Arabidopsis thaliana* genome (Deeks *et al.* 2003). All

these reports are evidences that the WAVE/SCAR regulation pathway exists in plants but it is still unclear if the regulatory mechanisms are conserved as well (Figure 19).

Nevertheless, the cloning of *GRL* and its protein interaction with other proteins suggests that the ternary complex is functionally conserved in plants.

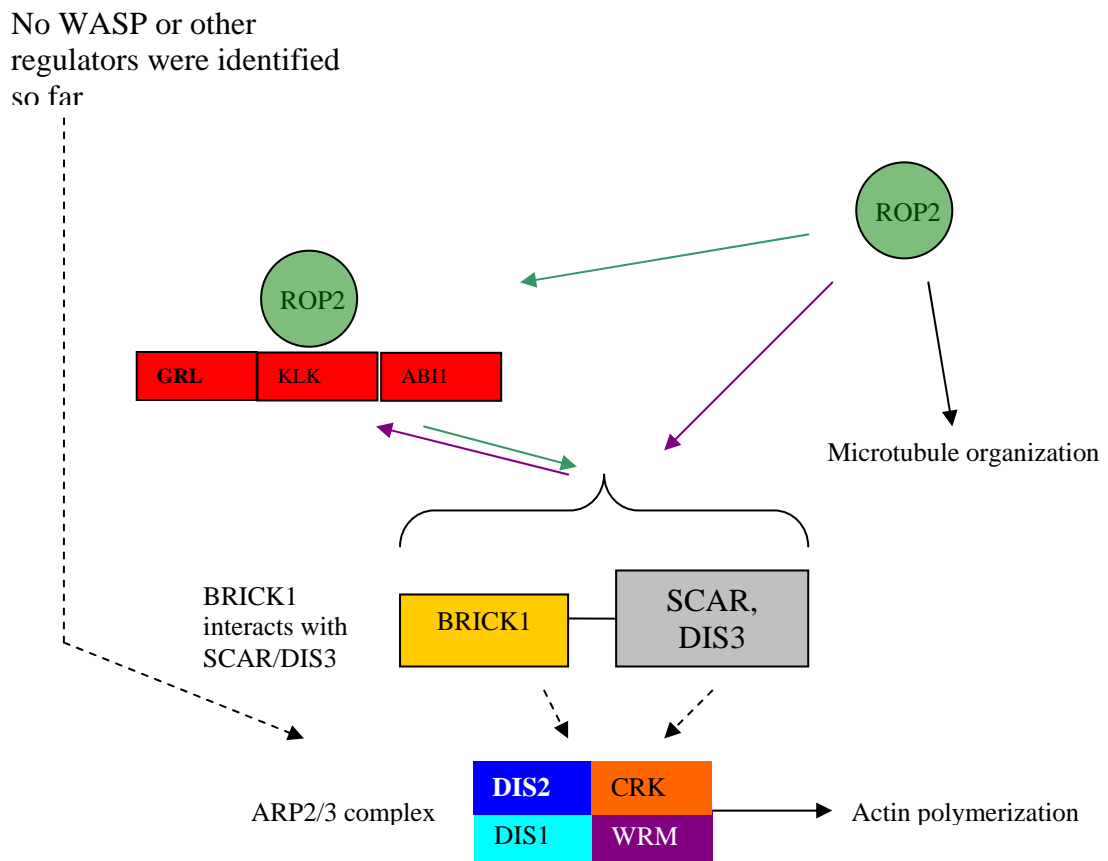


Figure 19. Schematical drawing of proposed pathways for ARP2/3 regulation in plants. Black arrows show known interactions, dashed lines show unknown interactions. Green arrows indicate the activation model of GRL, in which the binding of ROP2 activates the SCAR/DIS3 to activate again the ARP2/3 complex. The purple arrows represent the inhibition model in which ROP2 binding releases the ternary complex with GRL and allows the BRICK1 and SCAR/DIS3 to activate the ARP2/3 complex. Components described in this study are highlighted in bold.

4.2.1 *grl* mutant phenotype

According to the model depicted in Figure 19, GRL is upstream of ARP2/3 and seems to control its function. Therefore it is not surprising that *grl* mutants display cellular defects similar to those of *arp2/3* mutants. Two different actin cytoskeleton alterations were observed for the *grl* mutant. One group described an abundant fine actin in *grl* mutants (Mathur *et al.* 1999), suggesting that GRL serves as a positive regulator; another group described with other markers an actin cytoskeleton phenotype like that observed in the *arp2/3* mutants (Szymanski *et al.* 1999, Brembu *et al.* 2004), suggesting that GRL serves as a negative regulator.

These different descriptions can be explained by two animal ARP2/3 regulation pathways, involving different composition of proteins. In the one regulatory pathway, the ternary complex consisting of PIR121, NAP125 and Abi2 acts as a repressor of the HSPC300/WAVE1 complex and, upon binding of a Rho-like GTPase, HSPC300 and WAVE1 are released and the ARP2/3 complex is activated (Eden *et al.* 2002). In case that the regulatory mechanisms are comparable, the absence of NAP125 in the *grl* mutant should lead to an over-activation of the ARP2/3 complex and an increased amount of fine actin. On the other hand, in animals with a different set of proteins, WAVE2 appears to be activated by ABI1, NAP125 and PIR121, and re-localization upon RAC activation leads to a region-specific activation of the ARP2/3 complex (Miki *et al.* 2000, Innocenti *et al.* 2004).

While the abundant fine actin supports the first model, the vacuole phenotype of the *grl* mutant, which is similar to that observed in the *arp2/3* mutants, rather facilitates the second scenario, as bundled actin and abundant fine actin would supposedly promote different intracellular phenotype. The fact that different actin configurations are observed with different methods necessitates a direct comparison of the actin cytoskeleton in the *arp2/3* mutants and the *grl* mutant based on different approaches.

In many non-plant organisms, the loss of a single ARP2/3 subunit or a protein involved in the WAVE/SCAR pathway can be lethal (Winter *et al.* 1999, Hudson and Cooley 2002, Stevenson *et al.* 2002, Zallen *et al.* 2002, Sawa *et al.* 2003, Yan *et al.* 2003) whereas mutations in homologous plants genes are not. This offers two suggestions for the plant system: A) general redundancy for all WAVE/SCAR pathway proteins or B) the WAVE/SCAR pathway is not the major pathway for actin filament nucleation and other

proteins may play a more important role in actin nucleation. Potential candidates could be the FORMINs (Deeks *et al.* 2002) another class of potent actin nucleators, as speculated by some groups (Le *et al.* 2003, El- Assal *et al.* 2004a). This is supported by a recent publication in which the loss of one FORMIN protein, ATFH5, compromises cytokinesis in seed endosperm (Ingouff *et al.* 2005).

These suggestions show that plant cell growth or cell shape apparently is not primarily dependent on a WAVE/SCAR pathway. This becomes obvious from investigations of the *distorted* mutants, which reveal a reduced hypocotyl length and hypocotyl and root hair cells defects whereas the overall architecture of the plant and the cell remains normal. Trichomes, however, show the strongest effect of cell shape alteration by actin filament disturbance. The known *ARP2/3* genes and the *GRL* gene may therefore be essential to maintain a correct actin cytoskeleton that facilitates the intricate shape of the trichome cell.

4.3 SPIRRIG, an unknown component in cell shape regulation

As the *spirrig* mutant did not show an altered actin cytoskeleton (Schwab *et al.* 2003), like all the other *distorted* mutants (Mathur *et al.* 1999, Szymanski *et al.* 1999), its involvement in cell shape determination was of interest.

4.3.1 Spirrig mutant phenotype

The *spirrig* mutant was identified by its trichome phenotype (Hülkamp *et al.* 1994). As described before, the overall *spi* plant size is reduced like in other *arp2/3* mutants when compared to wild type. The stronger reduction in the *spi-4.2* allele may be explained by a second site mutation and is not considered to be allele specific.

Mutant trichomes are shorter than in wild type and the distortion is relatively weak. Moreover, the trichome branches are twisted and wavy. The second branching point of *spi* mutant trichomes is farther away from the first branching point than in wild-type

suggesting that growth is delayed in the mutant. This is also reflected in the smaller sized trichomes and their branches.

Comparing the trichome phenotype to other *distorted* mutants these aberrations are much more severe. The *dis2-1* mutant, for example, shows an additional swelling of the trichome, which is explained by the disruption of a direct nucleation factor of the actin cytoskeleton severely affecting the actin cytoskeleton and cell growth. The *grl* mutant shows smaller vacuoles. By contrast, the actin cytoskeleton and the vacuole in the *spi* mutant are indistinguishable from the wild type.

In addition, *spi* mutants also have slight altered epidermal pavement cells. Whereas in the wild type, these cells show a characteristic jigsaw-puzzle shape, pavement cells of *spi* leaves display rather spherical shapes. The fact that there is no difference between Col-0 and the T-DNA 205G08 might reflect the ecotype diversity. Other *distorted* mutants also featured a similar phenotype deviating from wild type. The reason for this phenotype is not yet understood. The alteration might depend on the way these cells grow, namely a mixture of tip and diffuse growth, and their attachment to other cells. Epidermal pavement cells are interconnected with neighboring cells except on their surface that is exposed to air. This contrasts completely with trichome cells, which are attached at their base to socket cells only. This isolation and non restriction of interconnecting cells might be the reason that growth defects in the mutant are much stronger in this cell type.

The hypocotyl of *spi* plants is reduced and some cells are detached and curl out from each other when grown under low-light conditions, leading to enhanced cell elongation. This is a common feature of all investigated *distorted* mutants so far. The reason of the detachment is not yet understood. However, in the mutants, cell growth rate is reduced resulting in smaller hypocotyls; the detached and curling out phenotype of the cells, however, can not be explained by this. Instead it could be suggested that under challenging growth conditions, the intracellular growth velocities on different sides of the cell is altered. The outer surface may grow slower, while the inner side grows with the same growth rate than the endodermal cells. By this, the outer cell wall might be shortened in length and therefore result in a curling out cell. Altered intracellular growth rates might also explain the slight twisting of the trichome branches in the *spi* mutant. Molecular experimental support is currently missing.

Roots of *spi* mutants present a striking root hair phenotype, like *centipede-1* (*cen1*) (Parker *et al.* 2000), which also showed the characteristic short root hair phenotype. Rough mapping localized *CEN1* on the upper arm of chromosome I, in the same region like *SPI*. The *cen1* mutant trichomes were described as wavy as the *spi* trichomes. Neither allelism tests nor cloning and DNA sequencing of the *CEN1* locus was reported thus far (Parker *et al.* 2000).

In a wild type plant, when root hairs have no contact to the nutritive medium, growth is induced to enable the plant to reach the nutrients. A rapid tip growth of root hair cells leads to elongated cells. Under the same conditions, the *spi* mutant cells are extremely short. Comparisons to other distorted mutants revealed that *spi* have the most prominent reduction of root hairs. Investigations concerning why the elongation defect is stronger in *spi* than in the other *distorted* mutants are missing. It is tempting to speculate that *SPI* is predominantly involved in tip growth, whereas the other proteins of the 'DISTORTED family' might play a stronger role in diffuse growth.

Vesicles or organelles, such as chloroplasts (Sheahan *et al.* 2004), peroxisomes (Mathur *et al.* 2002), and Golgi stacks (Nebenfuhr *et al.* 1999) traveling on the actin cytoskeleton are needed to promote cell growth. A mutant with short root hairs and a defect in the phosphatidylinositol transfer proteins (PITPs), which regulate signaling interfaces between lipid metabolism and membrane trafficking, was found in *Arabidopsis thaliana* (Vincent *et al.* 2005). The protein localizes along the root hair plasma membrane and is enriched in discrete plasma membrane domains and in the root hair tip cytoplasm. Because *SPI* might act in a similar manner, it might be interesting to visualize the location of *SPI* in the cell and its incorporation in vesicle trafficking.

4.3.2 Identification of the *SPI* gene

Several attempts to clone *SPI* were used. First a map based cloning approach, restricted by the size of the mapping population and the number of available markers, was utilized, as well as a tilling approach. Both methods did not allow cloning of *SPI*. Based on the mapping result and the assumption that large genes display higher allele frequencies, a gene candidate approach allowed the successful isolation of the *SPI* locus. Several point

mutations in the *SPI* locus generating stop codons in different *spi* alleles, helped in the identification of the locus, which encoded a 3600 amino acid long protein featuring a BEACH and several WD40 domains at its C-terminus. All identified stop codons in the mutants are located before or within the BEACH/WD40 domain. Interestingly, all *spi* mutants revealed the same phenotype. This finding implies that the BEACH/WD40 domain exhibits a crucial role for the correct function of SPIRRIG, even if around 97 % of the protein exists in the some mutants (suggested by the presence of mRNA).

4.3.3 BEACH mutants in *Dictyostelium discoideum*

The group of BEACH proteins is found in all eukaryotes (Ward *et al.* 2000, Wang *et al.* 2002). The *Arabidopsis thaliana* genome harbors 5 groups of genes encoding proteins with a BEACH domain. The BEACH proteins can be grouped into five different classes with multiple members in each class (Figure 20) (Wang *et al.* 2002). The BEACH proteins in general show a large diversity in sequence and the function of most members is unknown, except for three BEACH proteins from which the cellular role is known in detail: BEIGE, LVSA and FAN (class I, class II and class III, respectively).

SPI and its close homolog, At4g02660, belong to class II (Figure 20). The LVSA protein was the first BEACH protein found in *Dictyostelium discoideum* during a cytokinesis screen (Kwak *et al.* 1999). Null mutants of *lvsA* have a complete defect in cytokinesis when the cells are in suspension culture but not when attached to a substrate indicating that cells have two alternative ways to divide (Uyeda *et al.* 2000). The cytokinesis defect is very similar to that seen in *D. discoideum* clathrin mutants (Gerald *et al.* 2001). This and other common similarities in the phenotype of the two mutants, *lvsA* and *clathrin*, strongly suggest that LVSA participates in a membrane trafficking pathway that also involves CLATHRIN. However, *clathrin* mutants have defects, which are not found in LVSA (Ruscetti *et al.* 1999, Niswonger *et al.* 1997). This emphasizes that CLATHRIN controls a broad set of membrane trafficking pathways, one of which requires LVSA during cytokinesis. However, is not yet understood how these two proteins are involved in cytokinesis exactly. One possible scenario is that LVSA controls the fusion of vesicles

arriving at the cleavage furrow during cytokinesis. These vesicles may deliver special material necessary for the completion of cytokinesis.

An additional role of LVSA is the function in the contractile vacuole during osmoregulation. LVSA associates with the membrane of contractile vacuoles, just when the vacuole reaches its maximal diameter. The protein stays attached to the vacuole until it has entirely contracted and detaches then into the cytoplasm (Gerald *et al.* 2002).

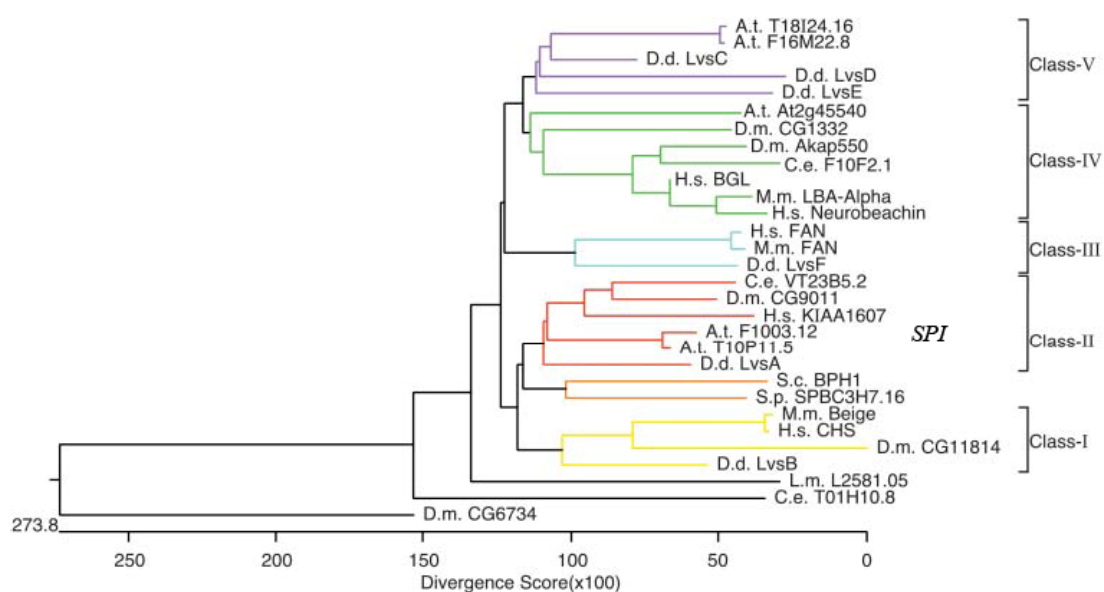


Figure 20. Phylogenetic tree of BEACH proteins. The BEACH and WD domains of the indicated sequences were aligned by the ClustalW algorithm and the alignment was used to construct this phylogenetic tree. Brackets indicate the different classes of BEACH proteins. A.t. F1003.12 represents SPI (modified from Wang *et al.* 2002).

4.3.4 Putative SPIRRIG protein function in *Arabidopsis thaliana*

The prediction of protein functions based on phenotype comparison of mutants belonging to different regna is always problematic. In the case of *SPIRRIG*, the *lvsA* phenotypes of *Dictyostelium discoideum* are difficult to compare to that of the *spi* mutant in *Arabidopsis thaliana*. The reported role of LVSA in osmoregulation can very likely be neglected because there is no contractive vacuole in plants. Furthermore, there is no hint of an altered vacuolization in the mutant based on the unchanged actin cytoskeleton.

The proposed LVSA function in the membrane trafficking process, combined with the function of PITP in the short root hair mutant, could provide a hypothetical function of SPI in membrane trafficking. SPI might be integrated by the seven predicted transmembrane domains in vesicles or in cell membranes and its BEACH/DW40 domain might be responsible for vesicles integration to the site of growth. This would hold true, if vesicles that are involved in growth and deliver cell material (Figure 18) as described before would be altered in the *spi* mutant. A localization analysis with fluorescence labeled SPI-protein, tracking of vesicles or organelles, or crossing fluorescence markers in the *spi* mutant background may give deeper insight into the localization of the protein and its possible function in membrane trafficking.

4.3.5 BEACH protein organization

All BEACH proteins have a similar structural organization. At the C-terminus they always have four to six WD40 repeats, which are predicted to fold into a beta-propeller structure that creates a protein-interaction domain. The BEACH domain is always vicinal on the N-terminal side. Whereas the WD40 domains share low sequence identity (around 20 %), the sequence in the BEACH domain is more conserved (around 50%-60% identity) (Lozanne 2003). The BEACH domain is comparably large (35 kDa) and might therefore represent more than a simple protein-interaction domain. It could e.g. harbor an enzymatic activity or facilitate a unique structural role. However, no such activity has been discovered so far. Even the 3-D structure of the mammalian neurobeachin (Jogl *et al.* 2002), gave no specific indication. The crystal structure revealed that the BEACH domain folds into a unique structure never observed in any other domain. The most unusual features of the domain are multiple segments that could neither be classified as beta-strands nor random coils.

No direct conclusions can be drawn from protein homology, but the importance and the uniqueness of the BEACH/WD40 domain *in planta* are clearly visible in the *spi* mutants. All stop codons found in the different *spi* alleles are upstream of the BEACH/WD40 domain or destroy the WD40 domain. This clearly demonstrates that the gene function depends on the presence of the entire protein. In the *spi-12* mutant allele, the mutation is just 117 amino acids away from the C-terminal end of the protein. Thus, the loss of information encoded in the last section seems crucial for the function. The *spi* mutants

could therefore be an intriguing assay system to investigate the specific role of the BEACH/WD40 domain. A vector with a BEACH/WD40 sequence could be introduced in different backgrounds ranging from the T-DNA knockout line to EMS mutants, in which different peptide pieces are present. The observed phenotype should be directly linked to the importance of the protein domains for partial or total rescue. Such a complementation should be visible in all affected cell types as the gene is expressed in all investigated plant tissues.

The *spi* mutant represents differences in trichome cell shape and root hair length compared to other *distorted* mutants. Analysis on the molecular level suggests that it might be a new component in cell growth.

Abstract

The leaf epidermal trichome of *Arabidopsis thaliana* is an ideal model system to study plant cell architecture due to its many mutants featuring *distorted* phenotypes. In this thesis, the *DISTORTED2* (*DIS2*), *GNARLED* (*GRL*) and *SPIRRIG* (*SPI*) genes were cloned and characterized. Both, the morphological as well as subcellular mutant phenotypes were assessed and discussed.

The *dis2* mutant displayed a pronounced distorted trichome phenotype, by having stubbed and swollen trichomes. The *DIS2* gene was cloned by a gene candidate approach and encoded the ARPC2 subunit of the actin nucleating protein 2 and 3 (ARP2/3) complex. Loss of function of the protein disclosed an aberrant actin cytoskeleton, when compared to wild type, and thus also featured an altered microtubule cytoskeleton. Based on the actin and microtubule density in the mutant and wild type, presumptions could be made of how local outgrowth of cells might be restricted to a defined area.

A similar trichome phenotype was observed in *grl* mutants. The *GRL* gene was identified through a gene candidate approach, revealing several mutations in the *GRL* gene. Protein homology analysis uncovered *GRL* as a homolog of the animal NAP125 protein. NAP125 is known to regulate the ARP2/3 complex. Phenotypical morphological analysis showed that *grl* exhibits the same plant defects, like pavement cell aberrations, hypocotyl cell and root hair defects, as observed in other *distorted* mutants. The cloning and identification of *GRL* suggested that the regulatory machinery to control the actin cytoskeleton is conserved in animals and plants.

The *spi* mutant disclosed similar plant defects as described above, but the trichome alterations were more subtle and the root hairs were shorter than those of wild type. Map based cloning attempts, gene candidate approaches and sequencing of several *spi* mutant alleles led to the identification of *SPI*. The *SPI* gene encoded a 3600 amino acids long protein, with seven transmembrane-, one BEACH- and four WD40- domains and is thus a novel protein in determining cell shape. Based on the *spi* phenotype as well as on the protein domains, mentioned above, a function in membrane trafficking could be suggested.

Zusammenfassung

Epidermale Blatthaare (Trichome) von *Arabidopsis thaliana* stellen durch ihre isolierte Position auf der Blattoberfläche, ein perfektes Modellsystem dar, um zellmorphologische Mutanten zu identifizieren. Drei „distorted“ Mutanten, *distorted2*, *gnarled* und *spirrig*, wurden sowohl phänotypisch als auch molekular charakterisiert und diskutiert.

Die *dis2* Mutante zeigte charakteristische „distorted“ Trichome, die klein und geschwollen waren. Die Klonierung des Gens erfolgte mittels eines Gen-Kandidaten-Klonierungsansatzes. Das *DIS2* Gen kodiert für die Untereinheit ARPC2 des „actin related protein 2 and 3“ (ARP2/3) Komplexes. Ein Funktionsverlust des Proteins führte zu einem veränderten Actin Zytoskelett. Diese Veränderung hatte auch Auswirkungen auf das Mikrotubulin Zytoskelett, das ebenfalls gegenüber dem Wildtyp verändert war. Aufgrund der unterschiedlichen Actin und Mikrotubulin Zytoskelettdichte, in der Mutante und im Wildtyp, konnten Vermutungen über den Prozess des Auswachsens eines definierten Bereiches einer Pflanzenzelle aufgestellt werden.

Die *grl* Mutante zeigte einen ähnlichen Blatthaar-Phänotyp, sowie Veränderungen anderer Zelltypen. Ein Gen-Kandidaten-Klonierungsansatz und die darauf folgende Sequenzierung mutanter Allele erlaubte die Identifizierung des *GRL* Gens. Das *GRL* Protein ist homolog zum tierischen *NAP125* Protein, das den ARP2/3 Komplex reguliert. Phänotypische morphologische Analysen zeigten, dass die *grl* Mutante dieselben Pflanzendefekte, wie veränderte epidermale Zellen, Hypokotyl- und Wurzelhaar- Defekte aufwies. Die Charakterisierung der *grl* Mutante und ihres Gens liessen vermuten, dass der regulatorische Apparat des Actin Zytoskelett in Pflanzen und Tieren sehr ähnlich ist.

Die *spi* Mutanten zeigten ähnliche Phänotypen wie die bereits beschriebenen, jedoch waren die Blatthaar-Defekte schwächer ausgeprägt und die Wurzelhaare kürzer als die des Wildtyps. Die Klonierung von *SPI* wurde durch eine genaue Kartierung des Lokus auf Chromosom I, sowie durch die Vielzahl der *spi* Allele ermöglicht. *SPI* codiert ein 3600 Aminosäure langes Protein mit sieben Transmembran-, einer BEACH- und vier WD40-Domänen und stellt dadurch ein neuartiges Protein in der Festlegung der Zellform dar. Basierend auf dem Mutanten Phänotyp und den vorhergesagten Proteindomänen, wurde eine Funktion von *SPI* im „membrane trafficking“ vermutet.

References

Alessa L, Kropf DL (1999). F-actin marks the rhizoid pole in living *Pelvetia compressa* zygotes. *Development* **126**: 201–209.

Altschul SF, Gish W, Miller W, Myers EW, Lipman DJ (1990). Basic local alignment search tool. *J Mol Biol* **215**: 403–410.

Ausubel F, Brent R, Kingston R, Moore D, Seidman J, Smith J, Struhl K (1994). *Current Protocols in Molecular Biology*.

Baluska F, Jasik J, Edelmann HG, Salajova T, Volkmann D (2000). Latrunculin B-induced plant dwarfism: Plant cell elongation is F-actin dependent. *Dev. Biol.* **231**: 113–124.

Baskin TI, Wilson JE, Cork A, Williamson, RE (1994). Morphology and microtubule organization in *Arabidopsis* roots exposed to oryzalin or taxol. *Plant Cell Physiol.* **35**: 935–942.

Baskin TI (2001). On the alignment of cellulose microfibrils by cortical microtubules: A review and a model. *Protoplasma* **215**: 150–171.

Basu D, El-Assal Sel-D, Le J, Mallery EL, Szymanski DB (2004). Interchangeable functions of *Arabidopsis* PIROGI and the human WAVE complex subunit SRA1 during leaf epidermal development. *Development* **131**: 4345–4355.

Basu D, Le J, El-Essal Sel-D, Huang S, Zhang C, Mallery EL, Koliantz G, Staiger CJ, Szymanski DB (2005). DISTORTED3/SCAR2 is a putative *Arabidopsis* WAVE complex subunit that activates the Arp2/3 complex and is required for epidermal morphogenesis. *Plant Cell* **17**: 502–24.

Bibikova TN, Blancaflor EB, Gilroy S (1999). Microtubules regulate tip growth and orientation in root hairs of *Arabidopsis thaliana*. *Plant J.* **17**: 657–665.

Blagg SL, Insall RH (2004). Solving the WAVE function. *Nat. Cell. Biol.* **6**: 279–281.

Blanchoin L, Amann KJ, Higgs HN, Marchand JB, Kaiser DA, Pollard TD (2000). Direct observation of dendritic actin filament networks nucleated by Arp2/3 complex and WASP/Scar proteins. *Nature* **404**: 1007–1011.

- Boevink P, Oparka K, Santa Cruz S, Martin B, Betteridge A, Hawes C** (1998). Stacks on tracks: the plant Golgi apparatus traffics on an actin/ER network. *Plant J.* **15**: 441-447.
- Brembu T, Winge P, Seem, M, Bones A.M** (2004). NAPP and PIRP encode subunits of a putative wave regulatory protein complex involved in plant cell morphogenesis. *Plant Cell.* **16**: 2335–2349.
- Carlier MF, Le Clainche C, Wiesner S, Pantaloni D** (2003). Actin-based motility: from molecules to movement. *Bioessays.* **25**: 336-345.
- Carol RJ, Dolan L** (2002). Building a hair: tip growth in *Arabidopsis thaliana* root hairs. *Philos. Trans. R. Soc. London B. Biol. Sci.* **357**: 815–821.
- Collings DA, Allen NS** (2000) Cortical actin interacts with the plasma membrane and microtubules. *In* Actin: A Dynamic Framework for Multiple Plant Cell Functions. 145–164. *Kluwer Academic Publishers*, Dordrecht.
- Clough SJ, Bent AF** (1998). Floral dip: a simplified method for agrobacterium-mediated transformation of *Arabidopsis thaliana*. *Plant J.* **16**: 735-743.
- Deeks MJ, Hussey PJ, Davies B** (2002): Formins: intermediates in signal-transduction cascades that affect cytoskeletal reorganization. *Trends Plant Sci.* **7**: 492-498.
- Deeks MJ, Hussey PJ** (2003). Arp2/3 and ‘the shape of things to come’. *Curr. Opin. Plant. Biol.* **6**: 561–567.
- Deeks MJ, Kaloriti D, Davies B, Malho R, Hussey PJ** (2004). *Arabidopsis* NAP1 is essential for Arp2/3-dependent trichome morphogenesis. *Curr. Biol.* **14**:1410-4.
- Dewitte W, Riou-Khamlichi C, Scofield S, Healy JM, Jacquard A, Kilby NJ, Murray JA** (2003). Altered cell cycle distribution, hyperplasia, and inhibited differentiation in *Arabidopsis* caused by the D-type cyclin CYCD3. *Plant Cell.* **15**: 79–92.
- Eden S, Rohtagi R, Podtelejnikov AV, Mann M, Kirschner MW** (2002). Mechanism of regulation of WAVE1-induced actin nucleation by Rac1 and Nck. *Nature* **418**: 790–793.
- El-Assal S, Le J, Basu D, Mallery EL, Szymanski DB** (2004). *Arabidopsis* GNARLED encodes a NAP125 homolog that positively regulates ARP2/3. *Curr. Biol.* **14**: 1405-9.

- El-Din El-Assal S, Le J, Basu D, Mallery EL, Szymanski DB** (2004). DISTORTED2 encodes an ARPC2 subunit of the putative Arabidopsis ARP2/3 complex. *Plant J* **38**: 526–538.
- Feenstra WJ** (1978). Contiguity of linkage groups 1 and 4, as revealed by linkage relationships of two newly isolated markers *dis-1* and *dis-2*. *Arab. Info. Serv.* **15**: 35–38.
- Folkers U, Berger J, Hülskamp M** (1997). Cell morphogenesis of trichomes in *Arabidopsis*: differential control of primary and secondary branching by branch initiation regulators and cell growth. *Development* **124**: 3779–3786.
- Folkers U, Kirik V, Schobinger U, Falk S, Krishnakumar S, Pollock MA, Oppenheimer DG, Day I, Reddy AS, Jürgens G, Hülskamp M** (2002). The cell morphogenesis gene ANGUSTIFOLIA encodes a CtBP/BARS-like protein and is involved in the control of the microtubule cytoskeleton. *EMBO J.* **21**: 1280–1288
- Frank MJ, Smith LG** (2002). A small novel protein highly conserved in plants and animals promotes the polarized growth and division of maize epidermal leaf cells. *Curr. Biol.* **12**: 849–853.
- Frank M, Egile C, Dyachok J, Djakovic S, Nolasco M, Li R, Smith LG** (2004). Activation of Arp2/3 complex-dependent actin polymerization by plant proteins distantly related to Scar/Wave. *Proc/Natl Acad Sci* **101**: 16379–16384.
- Fricker J** (2002). New assays for measuring prions reassure FDA. *Drug Discov Today* **7**: 537–539.
- Fu Y, Li H, Yang Z** (2002). The ROP2 GTPase controls the formation of cortical fine F-actin and the early phase of directional expansion during Arabidopsis organogenesis. *Plant Cell* **14**: 777–794.
- Fu Y, Gu Y, Zheng Z, Wasteneys G, Yang Z** (2005) Arabidopsis interdigitating cell growth requires two antagonistic pathways with opposing action on cell morphogenesis. *Cell* **120**: 687-700.
- Fukuda H** (2004). Signals that control plant vascular cell differentiation. *Nat. Rev. Mol. Cell Biol.* **5**: 379–391.
- Geldner N, Friml J, Stierhof Y-D, Jürgens G, Palme K** (2001). Auxin transport inhibitors block PIN1 cycling and vesicle trafficking. *Nature.* **413**: 425-428.
- Gerald N, Damer CK, De O'Halloran TJ, Lozanne A** (2001). Cytokinesis failure in clathrin-minus cells is caused by cleavage furrow instability. *Cell Motil Cytoskeleton* **48**: 213–223.

- Gerald N, De Siano M, Lozanne A** (2002). The *Dictyostelium* LvsA protein is localized on the contractile vacuole and is required for osmoregulation. *Traffic* **3**: 50–60.
- Giddings TH, Staehelin LA** (1991). Microtubule-mediated control of microfibril deposition: a reexamination of the hypothesis. In *The Cytoskeletal Basis of Plant Growth and Form*, C.W. Lloyd, ed. (Academic Press, London), pp. 85–99.
- Gilliland LU, Pawloski LC, Kandasamy MK, Meagher RB** (2003). Arabidopsis actin gene ACT7 plays an essential role in germination and root growth. *Plant J.* **33**: 319–328.
- Gu Y, Wang Z, Yang Z** (2004). ROP/RAC GTPase; an old master regulator for plant signaling. *Curr. Opin. Plant Biol.* **7**: 527–536.
- Hable WE, Miller NR, Kropf DL** (2003). Polarity establishment requires dynamic actin in fucooid zygotes. *Protoplasma* **221**: 193–204.
- Hawes CR, Satiat-Juenemaitre B** (2001). Trekking along the cytoskeleton. *Plant Physiol.* **125**: 119–122.
- Hayles J, Nurse P** (2001). A journey into space. *Nature Rev. Mol. Cell Biol.* **2**: 647–656.
- Hepler PK, Vidali L, Cheung AY** (2001). Polarized cell growth in higher plants. *Annu. Rev. Cell Dev. Biol.* **17**: 159–187.
- Higgs HN, Blanchoin L, Pollard TD** (1999). Influence of the C terminus of Wiskott–Aldrich syndrome protein (WASP) and the Arp2/3 complex on actin polymerization. *Biochemistry.* **38**: 15212–15222.
- Hudson AM, Cooley L** (2002). A subset of dynamic actin rearrangements in *Drosophila* requires the Arp2/3 complex. *J. Cell Biol.* **156**: 677–687.
- Hülkamp M, Misera S, Jürgens G** (1994). Genetic dissection of trichome cell development in *Arabidopsis*. *Cell* **76**: 555–566.
- Hülkamp M** (2004). Plant trichomes: a model for cell differentiation. *Nat. Rev. Mol. Cell Biol.* **5**: 471–480.
- Ingouff M, Gerald JN, Guerin C, Robert H, Sorensen MB, Damme DV, Geelen D, Blanchoin L, Berger F** (2005). Plant formin AtFH5 is an evolutionarily conserved actin nucleator involved in cytokinesis. *Nat Cell Biol.* **7**: 374–380.

- Innocenti M, Zucconi A, Disanza A, Frittoli E, Areces LB, Steffen A, Stradal TE, Di Fiore PP, Carlier MF, Scita G** (2004). Abi1 is essential for the formation and activation of a WAVE2 signalling complex. *Nat Cell Biol.* **6**: 319–327.
- Jogl G, Shen Y, Gebauer D, Li J, Wiegmann K, Kashkar H, Kronke M, Tong L** (2002). Crystal structure of the BEACH domain reveals an unusual fold and extensive association with a novel PH domain. *EMBO J.* **21**: 4785–4795.
- Kandasamy MK, McKinney EC, Meagher RB** (2002). Functional nonequivalency of actin isoforms in *Arabidopsis*. *Mol Biol Cell.* **13**: 251–261.
- Ketelaar T, de Ruitjer NCA, Emons AMC** (2003). Unstable F-actin specifies the area and microtubules direction of cell expansion in *Arabidopsis* root hairs. *Plant Cell* **15**: 285–292.
- Kim GT** (2002). The *ANGUSTIFOLIA* gene of *Arabidopsis*, a plant CtBP gene, regulates leaf-cell expansion, the arrangement of cortical microtubules in leaf cells and expression of a gene involved in cell-wall formation. *EMBO J.* **21**: 1267–1279.
- Kirik V, Mathur J, Grini PE, Klinkhammer I, Adler K, Bechtold N, Herzog M, Bonneville JM, Hulskamp M** (2002a). Functional analysis of the tubulin-folding cofactor C in *Arabidopsis thaliana*. *Curr. Biol.* **12**: 1519–1523.
- Kirik V, Grini PE, Mathur J, Klinkhammer I, Adler K, Bechtold N, Herzog M, Bonneville JM, Hulskamp M** (2002b). The *Arabidopsis* TUBULIN-FOLDING COFACTOR A gene is involved in the control of the alpha/ beta-tubulin monomer balance. *Plant Cell* **14**: 2265–2276.
- Kost B, Spielhofer P, Chua NH** (1998). A GFP-mouse talin fusion protein labels plant actin filaments in vivo and visualizes the actin cytoskeleton in growing pollen tubes. *Plant J.* **16**: 393–401.
- Kwak E, Gerald N, Larochelle DA, Vithalani KK, Niswonger ML, De Maready M, Lozanne A** (1999). LvsA, a protein related to the mouse beige protein, is required for cytokinesis in *Dictyostelium*. *Mol Biol Cell*, **10**: 4429–4439.
- Le J, El-Assal Sel-D, Basu D, Saad ME, Szymanski DB** (2003). Requirements for *Arabidopsis* ATARP2 and ATARP3 during epidermal development. *Curr. Biol.* **5**: 1341–1347.
- Li S, Blanchoin L, Yang Z, Lord EM** (2003). The putative *Arabidopsis* arp2/3 complex controls leaf cell morphogenesis. *Plant Physiol.* **132**: 2034–2044.

- Li Y, Sorefan K, Hemmann G, Bevan MW** (2004). Arabidopsis NAP and PIR Regulate Actin-Based Cell Morphogenesis and Multiple Developmental Processes. *Plant Phys.* **136**: 3616-27.
- Lozanne AD** (2003). The Role of BEACH Proteins in *Dictyostelium*. *Traffic* **4**: 6–12.
- Machesky LM, Atkinson SJ, Ampe C, Vandekerekhova J, Pollard TD** (1994). Purification of a cortical complex containing 2 unconventional actins from *Acanthamoeba* by affinity-chromatography on profiling agarose. *J Cell Biol* **127**: 107–115.
- Machesky LM, Insall RH** (1998). Scar1 and the related Wiskott–Aldrich syndrome protein, WASP, regulate the actin cytoskeleton through the Arp2/3 complex. *Curr Biol* **8**: 1347-1356.
- Machesky LM, Mullins RD, Higgs HN, Kaiser DA, Blanchoin L, May RC, Hall ME, Pollard TD** (1999). Scar, a WASp-related protein, activates nucleation of actin filaments by the Arp 2/3 complex. *Proc Natl Acad Sci USA*. **96**: 3739-3744.
- Marc J, Granger CL, Brincat J, Fisher DD, Kao T, McCubbin AG, Cyr R** (1998). A GFP-MAP4 reporter gene for visualizing cortical microtubule rearrangements in living epidermal cells. *Plant Cell* **10**: 1927–1939.
- Mathur J, Spielhofer P, Kost B, Chua NH** (1999). The actin cytoskeleton is required to elaborate and maintain spatial patterning during trichome cell morphogenesis in *Arabidopsis thaliana*. *Development* **126**: 5559–5568.
- Mathur J, Chua NH** (2000). Microtubule stabilization leads to growth reorientation in *Arabidopsis* trichomes. *Plant Cell* **12**: 465–477.
- Mathur J, Hülskamp M** (2002). Microtubules and microfilaments in cell morphogenesis in higher plants. *Curr. Biol.* **12**: 669–676.
- Mathur J, Hülskamp M** (2002b). Signal transduction: Rho-like proteins in plants. *Curr Biol.* **12**: R526-R528.
- Mathur J, Mathur N, Hülskamp M** (2002). Simultaneous visualization of peroxisomes and cytoskeletal elements reveals actin and not microtubule-based peroxisome motility in plants. *Plant Physiol.* **128**: 1031–1045.
- Mathur J, Mathur N, Kernebeck B, Srinivas BP, Hülskamp M** (2003a). Mutations in actin-related proteins 2 and 3 affect cell shape development in *Arabidopsis*. *Plant Cell* **15**: 1632–1645.

- Mathur J, Mathur N, Kirik V, Kernebeck B, Srinivas BP, Hülskamp M** (2003b). *Arabidopsis CROOKED* encodes for the smallest subunit of the ARP2/3 complex and controls cell shape by region specific fine F-actin formation. *Development* **130**: 3137–3146.
- Mathur J, Mathur N, Kernebeck B, Srinivas BP, Hülskamp M** (2003c). A novel localization pattern for an EB1-like protein links microtubule dynamics to endomembrane organization. *Curr. Biol.* **13**: 1991–1997.
- Mathur J** (2004). Cell shape development in plants. *Trends Plant Sci.* **9**: 583–590.
- Meagher, R.B. et al.** (2000). The significance of diversity in the plant actin gene family. In *Actin: A Dynamic Framework for Multiple Plant Cell Functions* (Staiger, C.J. et al., eds), pp. 3–28, Kluwer
- Miki H, Yamaguchi H, Suetsugu S, Takenawa T** (2000). IRSp53 is an essential intermediate between Rac and WAVE in the regulation of membrane ruffling. *Nature* **408**: 732–735.
- Mullins RD, Kelleher JF, Xu J, Pollard TD** (1998). Arp2/3 complex from *Acanthamoeba* binds profilin and cross-links actin filaments. *Mol Biol Cell.* **9**: 841-852.
- Murashige T, Skoog F** (1962). A revised medium for rapid growth and bioassays with tobacco tissue cultures. *Physiologia plantarum* **15**: 473-497.
- Nadeau JA, Sack FD** (2003). Stomatal development: cross talk puts mouths in place. *Trends Plant Sci.* **8**: 294-299.
- Nebenfuhr A, Gallagher LA, Dunahay TG, Frohlick JA, Mazurkiewicz AM, Meehl JB, Staehelin LA** (1999). Stop-and-go movements of plant Golgi stacks are mediated by the acto-myosin system. *Plant Physiol.* **121**: 1127-1142.
- Nesi N, Debeaujon I, Jond C, Pelletier G, Caboche M, Lepiniec L** (2000). The TT8 gene encodes a basic helix-loop-helix domain protein required for expression of DF and BAN genes in *Arabidopsis* siliques. *Plant Cell* **12**: 1863–1878.
- Niswonger ML, O'Halloran TJ** (1997). Clathrin heavy chain is required for spore cell but not stalk cell differentiation in *Dictyostelium discoideum*. *Development* **124**: 443–451.
- Oppenheimer DG, Pollock MA, Vacik J, Szymanski DB, Ericson B, Feldmann K, Marks MD** (1997). Essential role of a kinesin-like protein in *Arabidopsis* trichome morphogenesis. *Proc. Natl. Acad. Sci. U. S. A.* **94**: 6261–6266

- Panchal SC, Kaiser DA, Torres E, Pollard TD, Rosen MK** (2003). A conserved amphipathic helix in WASP/Scar proteins is essential for activation of Arp2/3 complex. *Nat Struct Biol.* **10**: 591-598.
- Parker JS, Cavell AC, Dolan L, Roberts K, Grierson CS** (2000). Genetic Interactions during Root Hair Morphogenesis in Arabidopsis. *The Plant Cell* **12**: 1961–1974.
- Qiu, JL, Jilk R, Marks MD, Szymanski DB** (2002). The *Arabidopsis SPIKE1* gene is required for normal cell shape control and tissue development. *Plant Cell.* **14**: 101–118.
- Ringli C, Baumberger N, Diet A, Frey B, Keller B** (2002). ACTIN2 is essential for bulge site selection and tip growth during root hair development of *Arabidopsis*. *Plant Physiol.* **129**: 1464-1472.
- Robinson RC, Turbedsky K, Kaiser DA, Marchand JB, Higgs HN, Choe S, Pollard TD** (2001). Crystal structure of Arp2/3 complex. *Science.* **294**: 1679-1684.
- Rodriguez OC, Schafer AW, Mandato CA, Forscher P, Bement WM, Waterman-Storer CM** (2003). Conserved microtubule-actin interactions in cell movement and morphogenesis. *Nat. Cell Biol.* **5**: 599–609.
- Rohatgi R, Ho HH, Kirschner MW** (2000). Mechanism of N-WASP activation by CDC42 and phosphatidylinositol 4,5-bisphosphate. *J Cell Biol.* **150**: 1299-1309.
- Rosso MG, Li Y, Strizhov N, Reiss B, Dekker K, Weisshaar B** (2003). An *Arabidopsis thaliana* T-DNA mutagenized population (GABI-Kat) for flanking sequence tag-based reverse genetics. *Plant Mol. Biol.* **53**: 247– 454.
- Ruscetti T, Cardelli JA, Niswonger ML, O’Halloran TJ** (1994). Clathrin heavy chain functions in sorting and secretion of lysosomal enzymes in *Dictyostelium discoideum*. *J Cell Biol.* **126**: 343–352.
- Saedler R, Mathur N, Srinivas BP, Kernebeck B, Hulskamp M, Mathur J** (2004a). Actin control over microtubules suggested by DISTORTED2 encoding the Arabidopsis ARPC2 subunit homolog. *Plant Cell Physiol* **45**: 813–822.
- Saedler R, Zimmermann I, Mutondo M, Hulskamp M.** (2004b) The Arabidopsis KLUNKER gene controls cell shape changes and encodes the AtSRA1 homolog. *Plant Molecular Biology* **56**: 775-782.
- Sawa M, Suetsugu S, Sugimoto A, Miki H, Yamamoto K, Takenawa T** (2003). Essential role of the *C. elegans* Arp2/3 complex in cell migration during ventral enclosure. *J. Cell Sci.* **116**: 1505–1518.

- Schaerer-Brodbeck C, Riezman H.** (2000). *Saccharomyces cerevisiae* Arc35p works through two genetically separable calmodulin functions to regulate the actin and tubulin cytoskeletons. *J Cell Sci* **113**: 521–532.
- Schneider K, Wells B, Dolan L, Roberts K** (1997). Structural and genetic analysis of epidermal analysis of epidermal cell differentiation in *Arabidopsis* primary roots. *Development* **124**: 1789–1798.
- Schwab B, Mathur J, Saedler R, Schwarz H, Frey B, Scheidegger C, Hülkamp M** (2003). Regulation of cell expansion by the *DISTORTED* genes in *Arabidopsis thaliana*: Actin controls the spatial organization of microtubules. *Mol. Gen. Genom.* **269**: 350–360.
- Sheahan MB, Rose RJ, McCurdy DW** (2004). Organelle inheritance in plant cell division: the actin cytoskeleton is required for unbiased inheritance of chloroplasts, mitochondria and endoplasmic reticulum in dividing protoplasts. *Plant J.* **37**: 379-390.
- Sieberer BJ, Timmers AC, Lhuissier FG, Emons AM** (2002). Endoplasmic microtubules configure the sub-apical cytoplasm and are required for fast growth of *Medicago truncatula* root hairs. *Plant Physiol.* **130**: 977–988.
- Smith LG** (2003). Cytoskeletal control of plant cell shape: getting the fine points. *Curr. Opin. Plant Biol.* **6**: 63–73.
- Stevenson V, Hudson A, Cooley L, Theurkauf W** (2002). Arp2/3-dependent pseudocleavage furrow assembly in syncytial *Drosophila* embryos. *Curr. Biol.* **12**: 705–711.
- Szymanski DB, Jilk RA, Pollock SM, Marks MD** (1998). Control of GL2 expression in *Arabidopsis* leaves and trichomes. *Development* **125**: 1161–1171.
- Szymanski DB, Marks DM, Wick SM** (1999). Organized F-actin is essential for normal trichome morphogenesis in *Arabidopsis*. *Plant Cell* **11**: 2331–2347.
- Szymanski DB, Lloyd AM, Marks MD** (2000). Progress in the molecular genetic analysis of trichome initiation and morphogenesis in *Arabidopsis*. *Trends Plant Sci.* **5**: 214-9.
- Tansengco ML, Imaizumi-Anraku H, Yoshikawa M, Takagi S, Kawaguchi M, Hayashi M, Murooka Y** (2004). Pollen Development and Tube Growth are Affected in the Symbiotic Mutant of *Lotus japonicus*, *crinkle*. *Plant and Cell Physiology* **45**: 511-520.

- Till BJ, Reynolds SH, Greene EA, Codomo CA, Enns LC, Johnson JE, Burtner C, Odden AR, Young K, Taylor NE, Henikoff JG, Comai L, Henikoff S** (2003). Large-scale discovery of induced point mutations with high-throughput TILLING. *Genome Res.* **13**: 524-30.
- Twell D, Park SK, Hawkins TJ, Schubert D, Schmidt R, Smertenko A, Hussey PJ** (2002). MOR1/GEM1 has an essential role in the plant-specific cytokinetic phragmoplast. *Nat. Cell Biol.* **4**: 711–714.
- Uyeda TQ, Kitayama C, Yumura S** (2000). Myosin II-independent cytokinesis in *Dictyostelium*: its mechanism and implications. *Cell Struct Funct.* **25**: 1–10.
- Van Gestel K, Kohler RH, Verbelen JP** (2002). Plant mitochondria move on F-actin, but their positioning in the cortical cytoplasm depends on both F-actin and microtubules. *J. Exp. Bot.* **53**: 659–667.
- Vartiainen MK, Machesky LM** (2004). The WASP-Arp2/3 pathway: genetic insights. *Curr Opin Cell Biol.* **16**: 174–181.
- Vernoud V, Horton AC, Yang ZB, Nielsen E.** (2003). Analysis of the small GTPase gene superfamily of *Arabidopsis*. *Plant Physiol.* **131**: 1191–1208.
- Vincent P, Chua M, Nogue F, Fairbrother A, Mekeel H, Xu Y, Allen N, Bibikova TN, Gilroy S, Bankaitis VA** (2005). A Sec14p-nodulin domain phosphatidylinositol transfer protein polarizes membrane growth of *Arabidopsis thaliana* root hairs. *J Cell Biol.* **168**: 801-12.
- Volkman N, Amann KJ, Stoilova-McPhie S, Egile C, Winter DC, Hazelwood L, Heuser JE, Li R, Pollard TD, Hanein D** (2001). Structure of Arp2/3 complex in its activated state and in actin filament branch junctions. *Science.* **293**: 2456-2459.
- von Groll U, Altmann T** (2001). Stomatal cell biology. *Current Opinion in Plant Biology* **4**: 555-560.
- Wang N, De Wu WI, Lozanne A** (2002). BEACH family of proteins: phylogenetic and functional analysis of six *Dictyostelium* BEACH proteins. *J Cell Biochem.* **86**: 561–570.
- Ward DM, Griffiths GM, Stinchcombe JC, Kaplan J** (2000). Analysis of the lysosomal storage disease Chediak–Higashi syndrome. *Traffic* **1**: 816–822.
- Wasteneys G O** (2002). Microtubule organization in the green kingdom: chaos or self order. *J. Cell Sci.* **115**: 1345-1354.

- Welch MD, DePace AH, Verma S, Iwamatsu A, Mitchison TJ** (1997). The human ARP2/3 complex is composed of evolutionarily conserved subunits and is localized to cellular regions of dynamic actin filament assembly. *J Cell Biol.* **138**: 375–384.
- Welch MD, Mullins RD** (2002). Cellular control of actin nucleation. *Annu Rev Cell Dev Biol.* **18**: 247-288.
- Whittington AT, Vugrek O, Wei KJ, Hasenbein NG, Sugimoto K, Rashbrooke MC, Wasteneys GO** (2001). MOR1 is essential for organizing cortical microtubules in plants. *Nature* **411**: 610–613.
- Winder SW** (2003). Structural insights into actin-binding, branching and bundling proteins. *Curr. Opin. Cell Biol.* **15**: 14-22.
- Winter D, Podtelejnikov AV, Mann M, Li R** (1997). The complex containing actin-related proteins Arp2 and Arp3 is required for the motility and integrity of yeast actin patches. *Curr Biol.* **7**: 519–529.
- Winter DC, Choe EY, Li R** (1999). Genetic dissection of the budding yeast Arp 2/3 complex: A comparison of the in vivo and structural roles of individual subunits. *Proc. Natl. Acad. Sci. USA* **96**: 7288–7293.
- Yang Z** (2002). Small GTPases: versatile signaling switches in plants. *Plant Cell* **14**:375–388.
- Yan C, Martinez-Quiles N, Eden S, Shibata T, Takeshima F, Shinkura R, Fujiwara Y, Bronson R, Snapper SB, Kirschner MW, Geha R, Rosen FS, Alt FW.** (2003). WAVE2 deficiency reveals distinct roles in embryogenesis and Rac-mediated actin-based motility. *EMBO J.* **22**: 3602–3612.
- Zallen JA, Cohen Y, Hudson AM, Cooley L, Wieschaus E, Schejter ED** (2002). SCAR is a primary regulator of Arp2/3-dependent morphological events in *Drosophila*. *J. Cell Biol.* **156**: 689–701.
- Zimmermann I, Saedler R, Mutondo M, Hülskamp M** (2004). The *Arabidopsis* *GNARLED* gene encodes the NAP125 homolog and controls several actin based cell shape changes. *Mol. Genet. Genomics.* **272**: 290–296.
- Zimmermann P, Hirsch-Hoffmann M, Hennig L, Gruissem W** (2004). GENEVESTIGATOR. *Arabidopsis* Microarray Database and Analysis Toolbox. *Plant Physiol.* **136**: 2621-2632.

Danksagung

Prof. Dr. Krämer möchte ich danken, dass er so bereitwillig die Betreuung der Arbeit übernommen hat, sowie für seine Berichterstattung.

Mein besonderer Dank gilt Prof. Dr. Hülkamp für die wissenschaftliche Betreuung, sowie für die Überlassung des wissenschaftlichen Themas, für seine stete Diskussionsbereitschaft, sowie für die Freiheiten mit der ich dieses Thema bearbeiten durfte. Vielen Dank auch für seine Berichterstattung.

Ganz speziell möchte ich Dr. Jaideep Mathur, der jetzt Professor in Guelph ist, für seine anfängliche Betreuung danken, die es mir ermöglichte, den Rest der Doktorarbeit so effizient zu gestalten. Ferner gilt mein Dank Neeta Mathur für die Zusammenarbeit.

Danken möchte ich Dr. Ilona Zimmermann and Moola Mutondo, ohne die das so schnelle Publizieren von Daten nicht möglich gewesen wäre.

Danke an das große Labor, für das angenehme Klima, das es so einfach machte zu arbeiten. Speziellen Dank geht an Birigt Kernebeck für ihre Zusammenarbeit und dass ich ihr immer Fragen stellen konnte, die sie mir mit gesundem Sarkasmus beantwortete. Danke an meine beiden Labortischnachbarinnen, Elena Galiana-Jaime und Britta Müller, für den vielen Spaß und das angenehme Arbeiten. Elena Galiana-Jaime möchte ich ebenfalls für die Zusammenarbeit danken.

Dr. Viktor Kirik möchte ich für seine stete Bereitschaft über Wissenschaft zu diskutieren danken. Danke auch an Dr. Bhylahalli P. Srinivas für die Zusammenarbeit.

Ich möchte Marcella Santaella-Tenorio für viel Spaß und die Bereitstellung einiger RNA Proben danken.

Ich möchte allen im Lehrstuhl III der Botanik danken, für den Support und das angenehme Arbeitsklima.

Vielen Dank an die ‚International Max-Planck Research School‘ für die Finanzierung der Doktorarbeit. Besonders möchte ich ihrem Leiter Dr. Ralf Petri danken, der mich in allen Belangen mit Rat und Tat unterstützte. Danke sagen möchte ich auch meinen IMPRS Kollegen, mit denen ich immer viel Spaß hatte.

Vielen Dank an alle, die meine Doktorarbeit gelesen haben.

Ich möchte mich ganz herzlich bei denjenigen bedanken, die mir bei dem Gelingen meiner Doktorarbeit geholfen haben.

Erklärung

Ich versichere, daß ich die von mir vorgelegte Dissertation selbständig angefertigt, die benutzten Quellen und Hilfsmittel vollständig angegeben und die Stellen der Arbeit – einschließlich Tabellen, Karten und Abbildungen –, die anderen Werken im Wortlaut oder dem Sinn nach entnommen sind, in jedem Einzelfall als Entlehnung kenntlich gemacht habe; daß diese Dissertation noch keiner anderen Fakultät oder Universität zur Prüfung vorgelegen hat; daß sie – abgesehen von unten angegebenen Teilpublikationen – noch nicht veröffentlicht worden ist sowie, daß ich eine solche Veröffentlichung vor Abschluß des Promotionsverfahrens nicht vornehmen werde. Die von mir vorgelegte Dissertation ist von Prof. Dr. Reinhard Krämer betreut worden.

Rainer Saedler

Teilpublikationen:

Saedler R, Mathur N, Srinivas BP, Kernebeck B, Hülskamp M, Mathur J (2004) Actin control over microtubules suggested by DISTORTED2 encoding the Arabidopsis ARPC2 subunit homolog. *Plant Cell Physiol.* **45**: 813–822.

Zimmermann I, Saedler R, Mutondo M, Hülskamp M. (2004) The Arabidopsis GNARLED gene encodes the NAP125 homolog and controls several actin-based cell shape changes. *Mol Genet Genomics.* **272**: 290-6.

Lebenslauf

Name Rainer Heinrich Franz Saedler
Adresse Mannsfelderstrasse 43
 50968 Köln
Email rainer@saedler.de
Geburtstag 01.06.1976
Geburtsort Freiburg i. Br., Deutschland

Ausbildung

09/82	-	07/86	Grundschule
09/86	-	03/95	Gymnasium
06/95			Allgemeine Hochschulreife
10/96	-	07/98	Biologiestudium an der Universität zu Köln, Deutschland
09/98			Vordiplom
10/98	-	07/00	Hauptfächer: Genetik und Biochemie Nebenfach: Organische Chemie
07/99	-	11/99	Praktikum am Max-Planck-Institut für Züchtungsforschung in Köln Thema: "Contributions to create a specific <i>Arabidopsis thaliana</i> MYB-Microarrays." Prof. Dr Bernd Weisshaar
03/00	-	05/00	Praktikum an der Universität von Minnesota im Institut der Pflanzenbiologie Thema: "Interaction of heat-shock-proteins." Prof. Dr. Robert Bramble
10/00			Diplomprüfungen
02/01	-	12/01	Externe Diplomarbeit an dem Max-Planck-Institut für Chemische Ökologie in Jena, Deutschland Thema: "Development of a virus induced gene silencing (VIGS) tool in <i>Nicotiana attenuate</i> " Prof. Dr. Ian Baldwin
12/01			Grad des Diplom Biologen
09/02	-	08/05	International Max-Planck Research School (IMPRS) Stipendium "The molecular basis of plant development and environmental interactions"
09/02			Doktorarbeit am Botanischen Institut der Universität zu Köln Thema: "Role of <i>DISTORTED2</i> , <i>GNARLED</i> and <i>SPIRRIG</i> in cell morphogenesis of <i>Arabidopsis thaliana</i> ." Prof. Dr. Reinhard Krämer
06/05			Angestrebtes Ende der Doktorarbeit

Zusatzausbildungen

1983 – 1987	Flötenunterricht an der Rheinische Musikschule Köln
1987 – 1994	Klavierunterricht an der Rheinische Musikschule Köln
1994 – 1996	Klarinettenunterricht an der Rheinische Musikschule Köln
1983 – 1990	Tennisunterricht an der Deutschen Sporthochschule Köln
1995 – 1996	Zivildienst als MSHD „Mobiler Sozialer Hilfsdienst“ beim Lazarus-Hilfswerk e. V.
2000	Basis Kurs in Wirtschaftslehre